Menin maintains enhancer-promoter interactions in a leukemia-specific manner

Vassilena Sharlandjieva[1,2], Catherine Chahrour[1], Frederik H. Lassen[3], Joseph C. Hamley[1], Andreas Damianou[2,4], Nicholas Denny[1], Alastair L. Smith[1], Svenja S. Hester[2], Iolanda Vendrell[2], Ronald W. Stam[5], Marina Konopleva[6], Anindita Roy[1,7] James O. J. Davies[1], Nicholas T. Crump[8], Benedikt M. Kessler[2,4*] and Thomas A. Milne[1*]

[1] MRC Molecular Haematology Unit, MRC Weatherall Institute of Molecular Medicine, Radcliffe Department of Medicine, University of Oxford, Oxford OX3 9DS, UK.

[2] Target Discovery Institute, Centre for Medicines Discovery, Nuffield Department of Medicine, University of Oxford, Roosevelt Drive, OX3 7FZ Oxford, UK

[3] Big Data Institute, Nuffield Department of Medicine, University of Oxford, Oxford, UK

[4] Chinese Academy of Medical Sciences Oxford Institute, Nuffield Department of Medicine, University of Oxford, Roosevelt Drive, OX3 7BN Oxford, UK

[5] Princess Máxima Center for Pediatric Oncology, Heidelberglaan 25, 3584, Utrecht, The Netherlands

[6] Montefiore Einstein Cancer Center, Department of Oncology and Cell Biology, 1300 Morris Park Avenue, Bronx, NY 10461, USA.

[7] Department of Paediatrics, University of Oxford, Oxford OX3 9DU, UK.

[8] Hugh and Josseline Langmuir Centre for Myeloma Research, Centre for Haematology, Department of Immunology and Inflammation, Imperial College London, London W12 0NN, UK

*These authors jointly supervised this work.

Correspondence: benedikt.kessler@ndm.ox.ac.uk (B.M.K); thomas.milne@imm.ox.ac.uk (T.A.M.)

Abstract

Inhibition of the protein-protein interaction between the Mixed Lineage Leukemia (MLL/KMT2A) protein and the adapter protein Menin is a promising therapy for both high-risk *MLL*-rearranged and *NPM1*-mutant (NPM1c) acute leukemias. However, the exact function of Menin in transcription regulation remains unclear, limiting our understanding of the utility of Menin inhibitors. Here, we compared the transcriptional responses of MLL-AF4 and NPM1c leukemias to Menin inhibition. We observed broad, acute transcriptional dysregulation in MLL-AF4 cells, whereas NPM1c showed few targets directly regulated by Menin binding. Screening for Menin interacting proteins by co-immunoprecipitation followed by mass spectrometry revealed a greater enrichment for transcriptional regulators and elongation factors in MLL-AF4 cells compared to NPM1c cells, pointing to protein complex and cell context-specific activity. Finally, we used high-resolution Micro-Capture-C to demonstrate that Menin regulates intragenic enhancer activity and maintains enhancer-promoter contacts in MLL-AF4 cells but not in NPM1c cells. Together, our findings show that Menin exerts distinct transcriptional effects depending on the protein complex it associates with, which is key to understanding how patients respond transcriptionally to Menin inhibition in distinct disease contexts.

Introduction

Chromatin is the DNA/protein complex in the cell that influences both transcriptional activity and cell identity[1]. In leukemia, frequent mutations in chromatin-modifying proteins and transcription factors trigger oncogenic transcription, often hijacking endogenous machinery, which leads to the expansion of immature progenitor cells[2, 3]. As a result, epigenetic enzymes, including transcriptional repressors (EZH2, HDAC, LSD1) and activators (P300, bromodomain proteins, DOT1L) have become promising targets in hematological malignancies[4-6].

Menin is a chromatin adapter protein that has emerged as a key vulnerability in high-risk leukemia. Menin is a component of multiple complexes[7-10], but its best studied role is as a member of the Mixed Lineage Leukemia complex (MLL1 or MLL, also known as KMT2A), where it interacts directly with the N-terminus of MLL. Rearrangements of the *MLL* gene (*MLL*r) give rise to oncogenic fusion proteins sufficient to drive leukemia, and account for approximately 10% of acute leukemias overall but up to 90% of infant B acute lymphoblastic leukemia (ALL)[11-13]. Patients with *MLL* rearrangements have a worse prognosis and a poor response to conventional chemotherapy[14], highlighting an unmet clinical need. MLL fusion proteins (MLL-FPs), most commonly MLL-AF4 in infants and MLL-AF9 in adults[15], assemble a large protein complex, including Menin, which activates gene expression through both epigenetic and transcription elongation mechanisms[16-18]. Menin is essential for leukemia initiation in the presence of MLL-FPs, facilitating oncogenic transcription by stabilizing MLL-FPs at hematopoietic genes such as *MEIS1*[19].

Menin inhibitors disrupt the Menin-MLL/MLL-FP interaction and initially aimed to target *MLL*r leukemia[20]. However, they have also been found to be effective in acute myeloid leukemia (AML) with *NPM1* mutations[21-25]. Affecting 30% of patients, *NPM1* mutations are the most common genetic lesion in AML[26], meaning that Menin inhibition (MENi) has the potential to benefit a large group of patients. *NPM1* mutations are commonly frameshifts in the C-terminus that disrupt a nucleolar localisation signal[27-30]. They have a dual effect on the typically nucleolar nucleophosmin protein—a portion of the mutant protein ("NPM1c") aberrantly localizes to the cytoplasm, while a small proportion in the nucleus can function as a transcription activator by directly binding a subset of Menin-MLL target genes[21, 23]. NPM1c is associated with expression of the *HOXA/B* cluster and their co-factor *MEIS1*—similar to MLLr leukemias[31, 32].

Menin inhibitors cause loss of Menin binding at chromatin and downregulation of key MLL-FP and NPM1c targets[22, 33]. However, as Menin is part of distinct complexes in MLL*r* and NPM1c

leukemias, it is unclear what role Menin plays in transcription in these leukemia subtypes. Both MLL-FPs and NPM1c are transcriptional activators, binding at active promoters and spreading into gene bodies[24, 34]. In addition to promoters, MLL-FPs have also been shown to bind enhancers[35-38]—non-coding regulatory elements that modulate gene transcription from a distance[39]. The resulting aberrant enhancer activation is a key mechanism driving oncogenic gene expression programmes in *MLL*r leukemia[37, 38, 40]. While this implicates Menin in the maintenance of enhancer activity in the presence of MLL-FPs, Menin also binds a subset of enhancers in ER+ breast cancer cells with wildtype MLL—suggesting a possible role in enhancer function independent of MLL-FPs[41]. NPM1c binding outside promoters has also been reported[24], but whether it is functionally maintaining enhancer activity—and whether it requires Menin for this—remains unknown. Better understanding the role of Menin in transcription in different contexts could inform our interpretation of patient response, relapse and resistance in ongoing clinical trials (summarized in[42] and[43]).

In this paper, we show that MENi triggers large scale, acute transcriptional dysregulation in MLL-AF4 ALL cells but not in NPM1c AML cells, where gene expression changes are temporally delayed and restricted to fewer Menin targets. This difference correlates with a higher enrichment of transcription regulators and elongation factors in the Menin interactome in MLL-AF4 cells compared to NPM1c cells, suggesting a more central role in gene activation. Finally, we show that Menin binds intragenic enhancers in the presence of MLL-AF4 and facilitates enhancer-promoter contacts at key oncogenes, whereas in NPM1c cells, Menin activity is restricted to promoters. Together, our characterization of Menin activity in distinct leukemia subtypes demonstrates that the mechanism by which MENi disrupts oncogenic transcription is unique to unique to context-specific Menin function.

Results

Menin inhibition has distinct transcriptional effects in MLL-AF4 and NPM1c cells

Current models for the therapeutic function of MENi propose that disrupting the Menin-MLL interaction destabilizes MLL-FP and NPM1c binding at a subset of their target promoters, which in turn triggers decreased gene expression[44]. However, it is still not clear whether target genes are equally sensitive to loss of Menin in different contexts, as most studies of the effects of MENi report transcriptional changes after multi-day treatments[25, 33].

We sought to compare the effects of MENi on nascent transcription at a defined early timepoint, using SEM and OCI-AML3 cells as models of MLL-AF4 ALL and NPM1c AML respectively. As a comparison to a model of insensitivity to MENi, we used RCH-ACV cells, an E2A-PBX1-driven ALL cell line. After treatment with the Menin inhibitor VTP50469 (250 nM) for 24 hours, Menin binding was depleted from transcription start sites (TSS) genome-wide in each cell line (Extended Data Fig. 1a). Despite this, the cell lines showed distinct dynamics in their sensitivity to MENi in terms of cell viability. SEM cells were highly sensitive, with an IC50 of 45.5 nM recorded at 48 hours of MENi (Extended Data Fig. 1b). Despite their known dependence on Menin, OCI-AML3 cells did not reach IC50 even at the highest concentration of inhibitor (62.5 μM) tested at this timepoint, similar to the insensitive RCH-ACV cells. Conversely, when measuring the colony formation capacity over two weeks, both SEM and OCI-AML3 colony formation was inhibited completely with MENi (Extended Data Fig. 1C).

To explore what drives differences in the response time of SEM (MLL-AF4) and OCI-AML3 (NPM1c) cells, we used Transient Transcriptome RNA-seq (TT-seq) to evaluate the effect of 24 h MENi on transcription (Fig. 1a). We saw the most extensive transcriptional changes in SEM (MLL-AF4) cells, in line with their early sensitivity. MENi resulted in 1874 differentially expressed genes in SEM cells, the majority (1058) of which were downregulated. They included MLL-AF4 targets such as *FLT3, MEF2C* and *JMJD1C* [33] but not *HOXA9* or *MEIS1*. In the inhibitor-insensitive RCH-ACV (E2A-PBX1) cells, we observed more upregulated than downregulated genes, albeit with smaller log2 fold changes (Fig. 1a, Extended Data Fig. 1d), indicating that insensitive leukemia cells can have a subtle transcriptional response to MENi without an effect on cell survival. Despite the clear loss of Menin chromatin binding and their known sensitivity to MENi (Extended Data Fig. 1a, c), OCI-AML3 (NPM1c) cells did not display a strong transcriptional response at 24 h of inhibition, with only 103 differentially expressed genes (Fig. 1a). Of these, 72 were downregulated, including *MEIS1*, which is considered the critical Menin-dependent vulnerability in these cells[21, 23, 24]. This comparison highlights that loss of Menin binding does not necessarily lead to rapid disruption of transcription at its targets but

instead can have specific transcriptional consequences in both sensitive and insensitive cell lines.

To understand what distinguishes MENi-responsive genes in SEM and OCI-AML3 cells, we tested for an association between Menin promoter binding and differential expression. Downregulated genes had higher average Menin enrichment compared to upregulated or unchanged genes in SEM and RCH-ACV cells, but not OCI-AML3 cells (Fig. 1b). A significant association between the presence of a Menin peak at the promoter and gene downregulation was detected in SEM and RCH-ACV, but not in OCI-AML3 (Fig. 1). This suggests that Menin binding is more generally associated with transcription activation in SEM cells but not OCI-AML3 cells.

We next sought to test whether the differential response to MENi could be explained by distinct gene targets specific to each cell line. We intersected Menin-bound promoters and found that the majority (5507) of genes were bound by Menin in all three cell lines (Fig. 1d). Of these 5507 common genes, 626 were downregulated with MENi in at least one cell line, but the majority (468) were uniquely downregulated in SEM cells (Extended Data Fig. 1e). Comparing all Menin-bound genes showed that downregulated Menin targets tended to be cell line-specific (Fig. 1e), with 11 common targets in the inhibitor-sensitive SEM and OCI-AML3 cells. Upregulated genes were also mostly cell-line specific, with the largest overlap shared between SEM and RCH-ACV cells (Extended Data Fig. 1F). In summary, although a set of genes were bound by Menin in all cell types tested, this was not predictive of sensitivity to MENi across cell lines in terms of transcriptional response or leukemia survival.

To confirm that Menin binding in SEM and OCI-AML3 cells is reflective of its targets in MLL-AF4 and NPM1c leukemia, we used small cell number ChIPmentation[45, 46] to map Menin binding in two infant ALL patients with an MLL-AF4 fusion (“iALL28349” and “iALL863388”) and an adult AML with NPM1c (“NPM1c-AML”[47]). Genome-wide, Menin binding was correlated between patient samples and cell lines (Extended Data Fig. 1g), and promoters with strong Menin enrichment in SEM and OCI-AML3 cell lines also had higher levels of Menin binding in the respective patient samples (Extended Data Fig. 1h, i). Visualising Menin enrichment at *FLT3*, *ARID1B*, and *PHF10* confirmed that common promoter binding did not correspond to common transcriptional responses (Fig. 1f). Together, these results argue that the primary driver of the differential effects of MENi is the context-dependent regulation of target genes, rather than Menin occupancy at the gene promoter.

Decreased MLL-AF4 and NPM1c binding accounts for only a subset of differentially expressed genes

The larger transcriptional response to MENi in SEM (MLL-AF4) cells indicated that Menin has a more general co-activator function in the MLL-AF4 complex, in contrast with its function in OCI-AML3 (NPM1c) cells. However, previous work has shown larger transcriptional changes in OCI-AML3 cells at later timepoints than 24 h (4 – 11 days)[21, 23-25]. To test whether OCI-AML3 Menin targets have delayed transcriptional changes compared to SEM cells, even though Menin binding loss has similar temporal dynamics, we compared changes in gene expression at later timepoints (24-72 h) in OCI-AML3 cells, alongside earlier timepoints (6-24 h) in SEM cells.

Overall, more genes were differentially expressed at the later treatment timepoints in both SEM and OCI-AML3 cells (Fig. 2a, 24 h in SEM and 72 h in OCI-AML3), indicating that both cell types have early and late-responsive Menin targets. In SEM cells, a greater proportion of Menin targets became downregulated between 6 h and 24 h compared to upregulated, making up 41% of differentially expressed genes. In OCI-AML3 cells, Menin-bound genes made up a greater proportion of downregulated genes at 72 h of inhibition (332/572, 58%), but a similar number of Menin targets were upregulated (356). While this time course suggests a delay in the transcriptional dampening of some Menin targets in OCI-AML3 cells, it confirmed that Menin targets are not preferentially down-regulated in OCI-AML3 as they are in SEM cells.

We hypothesised that the difference in the timing of transcriptional changes in response to MENi may be linked to the differential loss of Menin-dependent complexes from chromatin in the different cell types. Menin is thought to stabilize MLL-AF4 and NPM1c chromatin binding and both these oncoproteins have been shown to activate genes by recruiting RNA polymerase II and transcription elongation factors[24, 48, 49]. Upon MENi, MLL-FPs and NPM1c lose binding at a subset of targets, accompanied by reduced gene expression[21, 24, 33]. To determine if there is a temporal connection between gene expression changes and complex stability, we performed a differential analysis of MLL-AF4 and NPM1c binding at the early and late timepoints of MENi, corresponding to initial and more established changes in transcription. We used an antibody targeting the N-terminus of the MLL-AF4 fusion, which is preserved with wildtype MLL, and therefore refer to MLL/MLL-AF4 interchangeably in the context of SEM cells.

In SEM cells, regions depleted of MLL-AF4 binding (cluster 1) after MENi were enriched for promoters with high levels of Menin binding, whereas regions that retained or gained

MLL/MLL-AF4 binding (cluster 2) had less initial Menin binding and included sites away from promoters (Fig. 2b, left, Extended Data Fig. 2a). Menin binding was not fully depleted at 6 h of MENi treatment and we observed a further decrease in the mean MLL/MLL-AF4 signal at the 24 h timepoint (Extended Data Fig. 2b). Similar to MLL-AF4, decreased NPM1c binding was associated with Menin loss, whereas regions that gained NPM1c binding initially lacked Menin binding and correlated with a subtle increase in wildtype MLL enrichment (Fig. 2b, right). NPM1c binding changes occurred primarily in promoters (Extended Data Fig. 2c), and while NPM1c loss was more consistent between treatment timepoints, NPM1c gain was more pronounced at 72 h (Fig. 2c, Extended Data Fig. 2d).

In SEM cells, MLL/MLL-AF4 gain reflected a relatively subtle increase at pre-existing binding sites, as seen in the gene body of *JUN*, compared to the dramatic loss of MLL at key target promoters such as *CDK6* (Fig. 2c, left). On the other hand, while the loss of NPM1c at promoters such as *IGF2BP2* was similarly marked, increased NPM1c at *ONECUT3* reflected the emergence of a new promoter binding site for NPM1c and MLL-wt (Fig. 2c, right).

To test for an association between MLL-AF4 and NPM1c promoter binding and gene expression changes, we correlated gene expression and MLL-AF4/NPM1c ChIPmentation peaks at the late MENi treatment timepoint. At a relatively small subset of genes, gene expression mirrored statistically significant changes in oncoprotein (Fig. 2d). At 24 h, only 16.1% (176/1058) of downregulated genes in SEM cells had a concordant MLL-AF4 decrease (Fig. 2d, left). Similarly, in OCI-AML3 cells, in which we detected a total of 62 NPM1c-bound gene promoters, 2.4% of downregulated genes had decreased NPM1c binding (14/572) at 72 h (Fig. 2d, right). Curiously, the dramatic upregulation of *ONECUT3,* linked to appearance of a novel peak of NPM1c binding, suggests that the NPM1c gain following MENi could initiate transcription at this locus. Redistribution of wildtype MLL binding was also correlated with a subset of differentially expressed genes (44 downregulated, 25 upregulated, Extended Data Fig. 2f) at 72 hours in OCI-AML3 cells.

Together, our data indicate that transcription in the MLL-AF4 context is more dependent on Menin binding compared to in the NPM1c context. The rapid transcriptional changes in SEM cells suggest that Menin binding may function as a more general transcription co-activator in these cells, including at genes that retain some MLL-AF4 binding following MENi for 24 hours. In contrast, the absence of a strong association between loss of Menin and immediate widespread gene expression changes in OCI-AML3 cells suggests that its function is more important in maintaining expression at fewer loci, a subset of which are genes where MENi is sufficient to disrupt NPM1c binding. Together, this suggests that Menin has a more direct role

in maintaining transcription activation in the context of MLL-AF4, while it has a more indirect role in transcription in the context of NPM1c binding. This difference likely explains the relative delay in transcriptional changes in NPM1c mutant cells.

Menin interactors point to its context-specific roles in transcription

Given that loss of MLL-AF4 or NPM1c binding in SEM or OCI-AML3 cells was only linked to downregulation at a small subset of target genes, we next asked whether Menin may be interacting with additional protein complexes to facilitate distinct transcriptional processes based on the leukemia context. To test this, we performed endogenous Menin immunoprecipitation from nuclear extracts followed by mass spectrometry (IP-MS) in SEM (MLL-AF4), OCI-AML3 (NPM1c), and RCH-ACV (E2A-PBX1) cells.

Most proteins we identified as statistically enriched (FDR < 0.01 compared to IgG controls) were detected in the Menin IPs of all three cell lines (1406), while the second largest set was shared by SEM and RCH-ACV cells (438), suggesting common interactors in ALL cells (Fig. 3a). When factoring in protein abundance, the interactomes of SEM and RCH-ACV cells clustered apart from OCI-AML3 cells (Fig. 3b). These differences were not entirely driven by differential protein expression, as we saw a high correlation between the nuclear proteomes (IP inputs) of these cell lines (Extended Data Fig. 3a).

To identify transcription regulatory complexes associated with Menin, we performed an enrichment analysis for protein complexes in the Corum database[50] for each cell line. As expected, we found known interactions with the MLL1 complex in all three cell lines (Fig. 3c, “MLL1-WDR5”). However, members of FACT, UPS22-SAGA, and MSH2/6 DNA repair machinery were specifically enriched in SEM (MLL-AF4) cells. The expression of these complex components was highly correlated in the nuclei of both SEM and OCI-AML3 cells (Extended Data Fig. 3b), indicating that the observed differential enrichment reflects interactions with Menin rather than simply differential expression between these cell lines.

To assess whether the transcription-associated complexes uniquely enriched in SEM (MLL-AF4) cells are also key for cell survival, we referenced DepMap gene effect scores for the genes making up these complexes. A lower gene effect score indicates a greater effect on cell viability, where a score of -1 represents the median of common essential genes[51]. Gene effect scores were highly correlated in SEM (MLL-AF4) and OCI-AML3 (NPM1c) cells, with a subset emerging as essential in both cell lines (Fig. 3d). The selective enrichment of these transcriptional activators in SEM cells indicates that Menin may be repurposed for additional

gene activation (or DNA repair activity), possibly by stabilising the co-operation of these complexes with the MLL-AF4 complex.

We have previously shown that MLL-AF4 and interacting complexes such as DOT1L, FACT and PAF1, which are traditionally associated with transcription elongation[52-54], can also regulate enhancer activity in SEM (MLL-AF4) cells[36, 37]. In our IP data, we found that the acetyltransferase P300, which regulates promoter and enhancer activity via H3K27ac[55, 56], was also more enriched in the Menin interactome in SEM (MLL-AF4) cells compared to OCI-AML3 (NPM1c) and RCH-ACV (E2A-PBX1) cells (Extended Data Fig. 3c). As such, we hypothesised that MLL-AF4 may also co-opt Menin for driving enhancer activation in co-operation with its unique interactome of transcriptional co-activators. We therefore next explored whether the distinct transcriptional responses of SEM and OCI-AML3 cells can be further linked to Menin activity at enhancers.

Menin regulates enhancer activity in MLL-AF4 cells

To investigate Menin activity at enhancers, we first annotated Menin ChIP-seq peaks based on their localization to promoters, intragenic and intergenic enhancers, and linked these sites to genes using the nearest TSS. This confirmed Menin binding at a subset of enhancers, although less frequently than its known enrichment at promoters (Fig. 4a). Using publicly available AutoCUT&Tag[57] and ChIP-seq data, we also confirmed Menin enrichment outside promoters in other *MLL*r cell lines (Extended Data Fig. 4a, b). Intragenic Menin binding at regions marked by H3K27ac was also observed in our primary patient cells (Fig. 4b).

Given that MENi did not affect the viability of RCH-ACV (E2A-PBX1) cells, we focused on comparing the activity of Menin-bound enhancers in the inhibitor-sensitive SEM (MLL-AF4) and OCI-AML3 (NPM1c) cells. We found that Menin-bound intragenic enhancers were enriched near downregulated genes in SEM cells but not OCI-AML3 cells (Fig. 4c). This link was stronger for intragenic enhancers compared to intergenic enhancers (Extended Data Fig. 4c); we also identified more genes linked to Menin-bound intragenic enhancers (807, 55% of genes with an intragenic enhancer) versus intergenic enhancers (220, 35% of genes with an intergenic enhancer) in SEM cells. This observation was in line with previous work showing that Menin can spread into gene bodies in the presence of MLL-AF4[34]. Intragenic Menin-bound enhancers linked to downregulated genes had higher levels of Menin and MLL/MLL-AF4 in SEM cells, and to a lesser extent in OCI-AML3 cells (Fig. 4d). H3K27ac levels were similar at unchanged genes (Fig. 4d). Upon MENi, intragenic enhancers had reduced MLL-AF4 / MLL

binding and, more subtly, H3K27ac (Fig. 4d). A similar effect was observed at Menin-bound intergenic enhancers (Extended Data Fig. 4d).

A key attribute of enhancers is physical proximity with their target promoters in the 3D organisation of the genome[58-60]. Therefore, annotating enhancers to the nearest TSS may not reveal the true target promoter; instead, high-resolution Chromatin Conformation Capture techniques are needed to reliably link enhancers and promoters. We have previously shown using Capture-C that enhancers occupied by the MLL-AF4 complex lose promoter contact upon knock-down or enzymatic inhibition[36, 37]. To test whether Menin binding also maintains enhancer-promoter contacts, we used the higher-resolution Micro-Capture-C (MCC)[61] to identify enhancer contacts for key gene promoters in SEM and OCI-AML3 cells. Our panel of promoter viewpoints included known MLL-AF4 and NPM1c targets, genes sensitive to MENi, and genes linked to Menin-bound enhancers using the nearest TSS annotation in both cell lines (Supplementary File 1, Extended Data Fig. 4e).

We filtered MCC peaks to those overlapping with H3K27ac to define putative functional promoter interactions. Menin was enriched at 69% of promoter interactions (MCC peaks) at 43 genes analysed in SEM (MLL-AF4) cells, but only 7.5% of interaction sites at 42 genes analysed in OCI-AML3 cells (Fig. 5a). The majority (46%) of Menin-bound enhancers in SEM cells were within introns, followed by MCC peaks in other promoters (37%). In contrast, Menin was primarily enriched in other promoter regions (57%) in contact with the OCI-AML3 (NPM1c) promoter viewpoints. This contrast emphasized that Menin function is primarily restricted to key promoters in OCI-AML3 cells, whereas intragenic spreading[34] in SEM cells can be linked to enhancer activity.

By stratifying promoter contact sites based on Menin enrichment, we saw that enhancer-promoter contacts (MCC peaks) with the highest levels of Menin occupancy also had higher MLL/MLL-AF4, H3K27ac, and NPM1c enrichment in both cell lines (Fig. 5c, Extended Data Fig. 5a). Upon MENi for 24 hours, MLL-AF4 binding and H3K27ac decreased at these Menin-high enhancers (cluster 1, Fig. 5c) in SEM cells. Conversely, in OCI-AML3 cells, H3K27ac and NPM1c remained unaffected at the Menin-enriched contacts (cluster 1, Fig. 5c), suggesting a unique sensitivity to MENi in SEM cells.

We next asked whether MENi for 24 hours affected the ability of enhancers to interact with target promoters. The *ARID1B* locus illustrated the differential effects of MENi on enhancer activity in SEM (MLL-AF4) and OCI-AML3 (NPM1c) cells (Fig. 5d, left). In SEM cells, there were two large Menin-bound intragenic enhancers (highlights 1 and 2) at which MENi

dramatically reduces the frequency of interactions, visualised by subtracting the MCC signal of the DMSO condition from the inhibitor treatment (track labelled “subtraction”). This was matched by loss of MLL-AF4 and H3K27ac, indicating a loss of enhancer activity. In contrast, these large Menin-bound intragenic enhancers were absent in OCI-AML3 cells (Fig. 5d, left). Instead, the *ARID1B* promoter interacts with sites upstream (highlights 3 and 4) and within the fourth intron (highlight 5), which have low levels of Menin and are unaffected by the inhibitor treatment. The collapse of the intragenic Menin-bound enhancers in SEM cells correlates with decreased *ARID1B* expression following MENi (Extended Data Fig. 5b), while expression remained unaffected in OCI-AML3 cells.

Similarly, the broad intragenic enhancer in the gene body of *PAN3*, which contacts the *FLT3* promoter in SEM cells, collapsed upon MENi (Fig. 5d, right, highlight 6). Although OCI-AML3 cells also have some Menin occupancy at this site, it does not contact the *FLT3* promoter with the same frequency as in SEM cells, nor is it sensitive to MENi. *FLT3* nonetheless decreases expression following MENi in both SEM and OCI-AML3 cells (Extended Data Fig. 5c), suggesting that in the latter Menin primarily facilitates transcription from the promoter. Another NPM1c target gene in OCI-AML3 cells which featured Menin-bound enhancers was *BAHCC1*, yet both enhancer activity (measured by H3K27ac and contact frequency), NPM1c binding, and gene expression are mostly retained with MENi (Extended Data Fig. 6a, b).

To quantify changes in enhancer-promoter interactions upon MENi across all the sampled viewpoints, we calculated the change in the mean count of unique ligation junctions at each interaction site (MCC peak). In SEM cells, 49 interaction sites had a significant change in interaction frequency (Mann Whitney U test, FDR q-value < 0.05); of the decreased interactions, 90% (39/43) overlapped with Menin binding (Fig. 6a, left). Overall, the mean change in promoter interactions with Menin-bound enhancers was more pronounced than at sites lacking Menin binding in SEM cells (Wilcoxon test p-value < 0.01), pointing to a specific Menin inhibitor-driven effect. Conversely, there were no significant changes in interactions in OCI-AML3 cells, including at Menin-bound sites, suggesting that Menin is dispensable for enhancer-promoter contacts in these cells.

Of the altered promoter contact sites in MLL-AF4 cells, the majority (61%) were within introns (Fig. 6b), further corroborating the unique dependence of a subset of intragenic enhancers on Menin binding. These altered contact sites are also bound by Menin in MLL-AF4 ALL patients, but not in OCI-AML3 cells or our adult NPM1c patient sample (Extended Data Fig. 6b). Given that MENi led to both decreased H3K27ac and MLL-AF4 at MCC peaks with high levels of Menin binding in SEM cells (Fig. 5b), we sought to examine the relationship between these

factors and interaction frequency. At decreased interaction sites (Fig. 6c, cyan data points), the loss of interactions correlated most with reduced MLL-AF4 enrichment—although this correlation was still weak (R^2 = 0.32). The low correlation with Menin loss could be explained by the uniform activity of MENi, which displaces Menin binding genome-wide. Prior to inhibition, decreased interaction sites had higher Menin enrichment relative to unchanged peaks (Fig. 6d), suggesting that these sites may be more sensitive to Menin levels to stabilise MLL-AF4 and contacts with the promoter.

To confirm that Menin-bound enhancer-promoter contacts were functional, we linked the most significant interaction change to gene expression and observed that downregulated genes were more likely to have a decreased enhancer-promoter contact in SEM (MLL-AF4) cells (Fig. 6e). Among the genes with a concordant decrease in enhancer contacts and expression were *ARID1B, FLT3, PROM1*, and *CDK6* (Fig. 6f)—key oncogenes at which the MLL-AF4 complex has previously been shown to sustain enhancer-promoter contacts[37,38], confirming that enhancer activation and maintenance of proximity is an important function of Menin in MLL-AF4 leukaemia.

Together, our data point to distinct Menin activity in MLL-AF4 and NPM1c acute leukemias in transcriptional activation and modulating enhancer activity (Fig. 7). In MLL-AF4 cells, Menin functions as a transcriptional co-activator, interacting with other transcriptional activators and with elongation complexes. At intragenic enhancers, Menin facilitates interactions with promoters, which could account for the greater transcriptional disruption observed with MENi compared to NPM1c cells. In contrast, in NPM1c AML cells, Menin loss has a restricted acute effect on transcription at small subset of target loci, likely due to a more indirect effect on stabilizing NPM1c binding rather than directly recruiting transcription elongation complexes. The differences in Menin protein complex composition in different cell types have a direct impact on the transcriptional response, and this likely underlies the overall slower response to MENi in NPM1c cells.

Discussion

Menin inhibition is a promising targeted therapy for high-risk *MLL*-rearranged and *NPM1*-mutant acute leukemias, which both depend on Menin for the expression of key genes and cell survival. However, our data highlight that the mechanism by which Menin affects aberrant transcription differs between the two diseases. Upon MENi, SEM cells (MLL-AF4) exhibited rapid transcriptional dysregulation, which affected thousands of genes, and loss of intragenic Menin-bound enhancer activity. On the other hand, OCI-AML3 cells (NPM1c) showed transcription changes in approximately a hundred genes at the same timepoint, while enhancer activity was unaffected; instead, gene expression was altered more gradually over a longer exposure to MENi. Therefore, the major contribution of Menin to transcription is highly context-dependent, and dictated by the specific protein complex it participates in.

Our Menin co-immunoprecipitations from SEM (MLL-AF4), OCI-AML3 (NPM1c), and RCH-ACV (E2A-PBX1) cells revealed that Menin interacts with transcription regulators with some cell-type specificity. This adds to a complex body of literature illuminating context-specific Menin interactions that can trigger either transcription activation or repression[9]. Focusing on transcription regulators, we found that P300 and the FACT complex were more enriched in the Menin interactome of SEM cells compared to OCI-AML3 cells. The stronger transcriptional response to MENi in SEM cells was also linked to a decrease of interactions between promoters and Menin-bound intragenic enhancers, which was absent in OCI-AML3 cells. Given that loss of either PAF1, FACT[37] or H3K79me2/3[36] can lead to decreased enhancer-promoter interactions at MLL-AF4-bound enhancers, these multiple vulnerabilities suggest that the overall stability of the MLL-AF4 complex, rather than one specific component, is key to the maintenance of these contacts and transcription. This points to a possible role for Menin in stabilizing these factors at enhancers in MLL-AF4 ALL cells.

Both MLL-FPs and NPM1c are transcriptional activators that require Menin binding at a subset of their target promoters. Wang *et. al.* (2023) showed that chromatin-associated NPM1c forms transcriptional hubs, which include elongation factor ENL, Menin, and RNA Polymerase II, through multivalent interactions[24]. However, they also showed that NPM1c did not alter chromatin or trigger new transcription when introduced de novo; rather it further upregulates genes with an established baseline expression. MLL-FPs on the other hand, in addition to maintaining expression of active genes via the recruitment of co-activators and elongation factors[48, 62] can also activate self-renewal genes characteristic of hematopoietic stem cells when exogenously expressed[63]. More recently, it was demonstrated that MLL-AF10 can activate new enhancer elements[40]. Therefore, destabilizing MLL-AF4—a more potent and

wide-spread transcriptional activator compared to NPM1c—via MENi is likely more disruptive to the oncogenic gene expression programme, indicating that that Menin is co-opted as a transcriptional activator to a greater extent than when in a complex with NPM1c. Taken together with our results, this all suggests that Menin likely has very little independent function in mediating transcription, and context is essential for determining whether Menin is functioning as a strong activator or not.

While our analysis focused on MLL-AF4 ALL, it has also previously been observed that leukaemia cell identity can dictate the response to MENi. Comparing 4-day treatments with Revumenib in MLL*r* AML and ALL cells has revealed that MENi rapidly induces apoptosis and cell cycle arrest in MLLr-ALL cells, whereas in MLL*r*-AML cells the response is slower and involves differentiation rather than cell death[64]. Therefore, understanding Menin activity in the presence of both different driver mutations and in different leukaemia subtypes is key to extending MENi as a therapeutic option to the right patient populations[65]. Following evidence that Menin can regulate the transcriptional activity of NUP98 fusion proteins[66] and oncoproteins arising from *UBTF* tandem duplications[67], patients with these lesions are now included in Menin inhibitor clinical trials (e.g. NCT05326516, NCT05360160, NCT04811560, NCT06177067, APAL2020K ITCC-101/COG/PEDAL). Unexpectedly, Menin and its interacting complexes are also an emerging vulnerability in solid tumors[68, 69]. How Menin regulates genes in cancers with other driver mutations, and whether its function is goes beyond supporting the binding of other oncoproteins on chromatin, remains to be elucidated.

Monitoring the transcriptional responses to MENi over time could also be key to classifying patient responses as we ascertain resistance mechanisms. The AUGMENT-101 clinical trial reported that mutations in the Revumenib binding pocket on Menin can restore Menin/MLL-FP binding and expression of MLL-FP target genes[70]. However, when resistance arose without new mutations, the leukemias persisted despite the expected downregulation of Menin targets. This suggests that some leukemias can cease to depend on the Menin/MLL-FP transcriptional program despite an initial and sustained response to MENi. Distinct transcriptional responses to MENi, and how they link to clinical outcomes, can therefore provide a rationale for subtype-specific combination therapies.

Acknowledgements

We thank Jerry McGeehan (Syndax Pharmaceuticals) for supplying the VTP50469 used in these experiments. V.S. was funded by the Wellcome Trust. A.D. and B.M.K. were supported by the Chinese Academy of Medical Sciences (CAMS) Innovation Fund for Medical Sciences (CIFMS), China (grant number: 2024-I2M-2-001-1). T.A.M. was supported by Medical Research Council (MRC, UK) Molecular Haematology Unit grant MC_UU_00029/6. The work was also supported by Blood Cancer UK grant 24016. A.R. is supported by a Wellcome Trust Clinical Research Career Development Fellowship (216632/Z/19/Z) and Medical Research Council (MRC, UK) Molecular Haematology Unit grant MC_UU_00029/7. Samples and data used in this study were provided by VIVO Biobank, supported by Cancer Research UK & Blood Cancer UK (Grant no. CRCPSC-Dec21\100003).

Author Contributions

T.A.M, N.T.C., B.M.K., and V.S. conceived the experimental design. V.S., A.D., S.S.H., and A.L.S. carried out experiments. V.S, C.C., F.H.L., and J.C.H. analyzed and curated the data. V.S., C.C, N.T.C., and T.A.M. interpreted the data and wrote the manuscript. N.D. contributed toward MCC experimental design. I.V and S.S.H. developed mass spectrometry methods. R.W.S., M.K., and A.R. provided primary patient material. B.M.K. and T.A.M., provided funding and supervision. All authors reviewed the manuscript.

Data Availability

Genomics data have been deposited in the Gene Expression Omnibus (GEO) as a series under the accession number GSE312345. Mass spectrometry data have been deposited to the ProteomeXchange Consortium via the PRIDE partner repository with the dataset identifier PXD071336. Publicly available cell line data and previously deposited patient data are available in GEO under accession codes: GSM5114291; GSM5139719; GSM5139645; GSM5139689; GSM8657204; GSM8657208; GSM8657184; GSM8657191; GSM5858383; GSM3635683.

Competing Interests

T.A.M. and N.T.C. are paid consultants for and shareholders in Dark Blue Therapeutics Ltd. F.H.L is a director and shareholder at Omos Biosciences Ltd. J.O.J.D is a founder of and consultant for Nucleome Therapeutics. The remaining authors declare no competing interests.

Methods

Cell culture

SEM cells (DSMZ) were grown in IMDM supplemented with 10% FBS and 1X GlutaMax (Gibco). RCH-ACV and OCI-AML3 (DSMZ) cells were grown in RPMI supplemented with 10% FBS and 1X GlutaMax (Gibco).

Patient samples

Infant (aged <1 year at diagnosis) ALL samples were obtained from Blood Cancer UK Childhood Leukaemia Cell Bank (now VIVO Biobank, United Kingdom) under their ethics approval (REC: 23/EM/0130) and from Our Lady's Children's Hospital, Crumlin, Ireland (REC: 21/LO/0195). The adult AML sample was obtained from MD Anderson Centre, USA, under RB protocol LAB-01-473.

CellTiterGlo

Cells were treated with a dilution series of VTP50469 fumarate (Syndax Pharmaceuticals) in triplicate wells in an opaque 96 well plate. After 48 h, CellTiterGlo 2.0 reagent (Promega G9241) was added to each well in equal volume to the media. The plate was shaken for 2 min and incubated for 5 min at room temperature, after which luminescence was recorded on a BMG FLUOstar OPTIMA plate reader. The luminescence signal was normalised to DMSO-treated cells and averaged across replicates. The dose response curves were fitted using the R package drc[71].

Colony Assay

In duplicate, cells were treated with either 50 nM or 250 nM VTP50469, or DMSO, for 90 min, then added to MethoCult (StemCell Technologies H4100) containing 50 nM or 250 nM VTP50469 or DMSO. Methocult cultures were aliquoted into three replicate 3 cm dishes, for a total of 5 replicate plates per condition. After 10-14 days, the number of colonies was counted under a light microscope and the counts across replicates were averaged.

Chromatin Immunoprecipitation followed by Sequencing (ChIP-seq)

For Menin, NPM1c and MLL-N ChIP, cells were fixed for 30 min with 2 mM Di(N-succinimidyl) glutarate (DSG) followed by 30 minutes with 1% formaldehyde. For histone modifications, cells were fixed for 10 minutes with 1% formaldehyde. Fixed cells were lysed in SDS lysis buffer (1% SDS, 10 mM EDTA, 50 mM Tris-HCl, pH 8 with protease inhibitor cocktail) and the lysate was syringe-passaged through a 27 gauge needle. The cell lysates were sonicated using a Covaris ME220 (peak power 75, duty factor 25 %, 500 cycles per burst) for 10 min for Menin,

NPM1c and MLL-N ChIP, or for 5 min for histone ChIP. The sonicated lysates were pre-cleared with a 1:1 mix of Protein A:Protein G beads for 15 minutes at 4˚C, then incubated with antibody overnight. Antibodies are provided in Supplementary Table 1. Five percent of the lysate was set aside as input. The following day, a 1:1 mix of Protein A:Protein G beads was added to each IP and samples were rotated at 4 ˚C for 3 hours. The beads were then washed three times with RIPA buffer (50 mM HEPES-KOH, pH 7.6, 500 mM LiCl, 1 mM EDTA, 1% NP-40, 0.7% Na-deoxycholate) and once with TE/50 mM NaCl. The chromatin was eluted from the beads with SDS lysis buffer for 30 min at 65 ºC, then treated with RNase A for 30 min at 37 ºC, followed by Proteinase K treatment combined with cross-link reversal overnight at 65 ºC. DNA was purified using the ChIP DNA Clean & Concentrator kit (Zymo 5201). Libraries for sequencing were prepared using the NEBNext Ultra II library prep kit (E7645) and sequenced by 40 bp paired-end sequencing with a NextSeq500 (Illumina).

ATAC-seq

ATAC-seq was performed as described by Buenrostro *et al*[72]. 50,000 cells were lysed in 50 µL cold lysis buffer (10 mM Tris-HCl pH 7.4, 10 mM NaCl, 3 mM MgCl2, 0.1 % IGEPAL CA-630) and centrifuged at 500 g for 10 minutes at 4°C. The pellet was resuspended in transposase buffer (1X Illumina Tagment DNA Buffer - 20034197) with 2.5 µL Tn5 Transposase enzyme and incubated for 30 min at 37°C. Transposed DNA was extracted using the MinElute PCR Purification Kit (Qiagen 28004) following the manufacturer's instructions, then PCR-amplified using Nexterra indices and NebNext Ultra II Q5 MasterMix (NEB M0544S) for a total of 12 cycles. Amplified tagmented DNA was purified with the MinElute PCR Purification Kit and sequenced by 75 bp paired-end sequencing.

Transient Transcriptome RNA-sequencing (TT-seq)

TT-seq was performed as previously described[73]. In triplicate, 4-5x10^7 cells were labelled with 500 µM 4-thiouridine (Sigma) for 5 min. 50 ng spike-in RNA, consisting of three 4-thiouridine-labelled transcripts from a CAS9-encoding vector, was added to each replicate. Total RNA was extracted with either Trizol or RNeasy Maxi kit (Qiagen), DNase I-treated, and fragmented by sonication on Covaris ME220 for 10 s (peak power 70 W, duty factor 20%, 1000 cycles/burst). 150-200 µg input RNA was labelled with EZ-Link HPDP-Biotin (Pierce 21341) for 90 min and purified by chloroform/isoamylalcohol extraction. Labelled RNA (i.e. nascent transcripts) was isolated using the uMACS Streptavidin Kit (Miltenyi 130-074-101) following the manufacturer's instructions and purified with the RNeasy MinElute Cleanup Kit (Qiagen 74204). cDNA synthesis and library preparation for sequencing were performed using the NEBNext Ultra II Directional RNA Library Prep Kit (NEB E7760) following the protocol for purified mRNA. The libraries were quantified using the KAPA Library Quantification Kit (Roche

KK4824) and sequenced by 80 bp paired-end sequencing or 150 bp paired-end sequencing with a NextSeq500 (Illumina).

ChIPmentation

ChIPmentation was performed as previously described[46]. Protein A magnetic beads were conjugated with 1.5 µg of antibody for 4 hours at 4 °C with rotation in 150 µL PBS 0.5% BSA 1 x protease inhibitor cocktail (PIC). Antibodies are provided in **Supplementary Table 1.** Cells were fixed as for ChIP-seq. Fixed cells were lysed in 120 µL Lysis Buffer (50 mM Tris-HCl pH 8.0, 0.5% SDS, 10 mM EDTA, 1x protease inhibitor cocktail (PIC) and sonicated using Covaris ME220 using the same conditions as for ChIP-seq to generate 200-300 bp fragments. Triton-X100 was added to the sonicated chromatin to a final concentration of 1% and incubated for 10 min at room temperature to neutralize the lysis buffer SDS. The chromatin was pre-cleared with protein A beads for 30 minutes at 4 °C with rotation. Antibody-conjugated beads were washed with 150 µL PBS 0.5% FBS, then added to the pre-cleared chromatin and incubated overnight at 4 °C with rotation. The following day the beads were washed three times with RIPA buffer (as in ChIP-seq), once with Tris-EDTA and once with 10 mM Tris-HCl pH 8.0. The beads were then resuspended in Tagmentation Buffer (10 mM Tris-HCl pH 8.0, 5 mM $MgCl_2$, 10% dimethylformamide) with 1 µL Tn5 transposase (Illumina). Samples were incubated at 37 °C for 5 minutes, after which the transposition reaction was stopped with 150 µL RIPA buffer. Beads were washed with 10 mM Tris-HCl pH 8.0. PCR was performed with NEBNext Ultra II Q5 Mastermix and Nextera index primers (125 nM final concentration) for 13 cycles. AMPure XP beads (Beckman A63881) in a 1:1 ratio were used for clean-up. Samples were sequenced with paired-end sequencing with a NextSeq500 (Illumina).

Immunoprecipitation

$4x10^7$ cells were lysed in 1 mL Buffer A (10 mM HEPES pH 7.9, 10 mM KCl, 1.5 mM $MgCl_2$, 0.34 M sucrose, 10% glycerol) with 0.2% NP-40 and 1x PIC for 5 minutes on ice. Following a 5 minute centrifugation at 500g and 4 °C, the cytoplasmic fraction (supernatant) was removed and intact nuclei were washed once in Buffer A + PIC. The nuclei were resuspended in Nuclear Lysis Buffer (50 mM Tris-HCl, pH 8, 2 mM $MgCl_2$, 150 mM NaCl, 0.5% NP-40, 1x PIC) with 250 U benzonase (Sigma) and rotated for 1 h at 4 ˚C. After centrifugation at 20,000 g for 10 min and 4 °C, 2% of the supernatant was set aside as a nuclear input and the remainder was used for immunoprecipitation with 4 µg anti-Menin antibody (Bethyl A300-105A) overnight at 4 °C. An equal amount of rabbit IgG antibody (Cell Signalling DA1E) was used in parallel as a control. A 1:1 mix of Protein A:Protein G beads was added to each IP and rotated at 4 °C for 3 h. The beads were washed three times with Nuclear Lysis Buffer and once with TE/50 mM NaCl. The beads were then resuspended in 35 µL 2X LDS buffer and proteins were eluted by

incubating at 95 °C for 5 min. For quality checks, approximately 4% of the sample was used for SDS-PAGE followed by Silver Stain (Pierce™ Silver Stain Kit, ThermoFisher 24612).

Mass Spectrometry

Peptides were prepared for Mass Spectrometry with the S-trap micro spin column digestion protocol (PROTIFI), following the manufacturer's instructions. Briefly, SDS was added to IP and nuclear inputs to a final concentration of 4%, after which samples were reduced, alkylated and acidified, then purified with the S-Trap micro column. After 5 washes with the binding/wash buffer, 5 µg Trypsin was added and columns were incubated at 37 °C overnight. Peptides were resuspended in 5% formic acid and 5% DMSO and then trapped on an Acclaim™ PepMap™ 100 C18 HPLC Columns (PepMapC18; 300µm x 5mm, 5µm particle size, Thermo Fischer) using solvent A (0.1% Formic Acid in water) at a pressure of 60 bar and separated on an Ultimate 3000 UHPLC system (Thermo Fischer Scientific) coupled to a QExactive mass spectrometer (Thermo Fischer Scientific). The peptides were separated on an Easy Spray PepMap RSLC column (75µm i.d. x 2µm x 50mm, 100 Å, Thermo Fisher) and then electro-sprayed directly into an QExactive mass spectrometer (Thermo Fischer Scientific) through an EASY-Spray nano-electrospray ion source (Thermo Fischer Scientific) using a linear gradient (length: 60 minutes, 5% to 35% solvent B (0.1% formic acid in acetonitrile and 5% dimethyl sulfoxide), flow rate: 250 nL/min). The raw data was acquired in the mass spectrometer in a data-independent mode (DIA). Full scan MS spectra were acquired in the Orbitrap (inclusion list with scan range 495 to 995 m/z, 20m/z increments, with an overlap of +/- 2 Daltons, resolution 35000, AGC target 3e6, maximum injection time 55ms). After the MS scans peaks were selected for HCD fragmentation at 28% of normalised collision energy (NCE) / stepped NCE. HCD spectra were also acquired in the Orbitrap (resolution 17500, AGC target 1e6, isolation window 20m/z).

Micro-Capture-C

Micro-Capture-C was conducted as previously[61, 74]. In triplicate, $5x10^7$ SEM and OCI-AML3 cells were treated with 250 nM VTP50469 or DMSO for 24 hours. Cells were fixed with 2% formaldehyde for 10 min, followed by quenching with glycine and a PBS wash. Cells were then aliquoted into three technical replicates. 0.0005% digitonin (Sigma) was used to permeabilize the cells for 15 minutes, after which they were snap frozen in three aliquots. After thawing, 16 x 10^6 cells (one aliquot) were resuspended in 10mM Tris-HCl pH 7.5, 1 mM $CaCl_2$ and divided into three micrococcal nuclease (NEB) digestion reactions with 7.5, 10 or 12.5 Kunitz U for 1 h at 37 °C shaking at 550 rpm in a Thermomixer (Eppendorf). MNase digestion was stopped with 5 mM EGTA and an aliquot was set aside to assess digestion by TapeStation. The cells were washed with PBS/5 mM EGTA and resuspended in: DNA ligase buffer, 400 µM dNTPs,

5 mM EDTA, 100 U/µL DNA Polymerase 1, Large (Klenow) Fragment (NEB), 200 U/µL T4 PNK (NEB) and 300 U/µL T4 DNA ligase (Thermo Scientific). This ligation reaction was incubated at 550 rpm at 37 °C for 2 h followed by 20 °C for 8 hours, then held at 4 °C in a ThermoMixer. Cells were then washed with PBS and digested with Proteinase K at 65 °C overnight to simultaneously reverse crosslinks. DNA was purified using phenol:chloroform:isoamyl alcohol (25:24:1) and digestion and ligation were assessed by TapeStation (Agilent D1000). 3C libraries (two technical replicates per biological replicate) were sonicated to 200 bp on Covaris ME220. Indexing was performed in duplicate using Illumina paired-end adapters, NEB Indices and Herculase II (Agilent). Enrichment for promoters of interest was performed twice with 120 nt biotinylated capture probes using the HyperCapture Target Enrichment Kit (Roche), using M270 streptavidin beads (Invitrogen) for the pulldown. Capture probes were designed using the Capsequm pipeline (https://github.com/Davies-Genomics-and-Genome-Editing-Lab/oligo_design_pipeline). Sequences are provided in Supplementary File 1. Samples were sequenced by 150 bp paired-end sequencing on NextSeq500 (Illumina).

Bioinformatic analysis

Publicly available genomics data was accessed from GEO. References to the data are provided in Supplementary Table 2.

ChIP-seq and ChIPmentation. Sequencing reads were trimmed using trim_galore (https://github.com/FelixKrueger/TrimGalore) and aligned to hg38 using bowtie2[75]. DeepTools[76] was used to create bigwig files for visualization on UCSC and to generate heatmaps and metaplots. HOMER[77] was used to call peaks using findPeaks and the flag -style histone. Differential peak analysis was performed with the R package DiffBind[78]. Heatmaps of differential peaks were generated with R package ComplexHeatmap[79].

TT-seq. Transient transcriptome RNA sequencing reads were aligned to human genome (hg38) using STAR[80] and gene expression levels were determined using the Subread package tool featureCounts[81]. Differential gene expression analysis was completed using edgeR[82]. Metaplot visualisations of strand-specific transcription were created using the deepTools command computeMatrix and plotted in R using ggplot2. χ^2 tests were performed using the R package ggstatsplot[83].

Genomic annotation. ATAC, ChIP-seq and ChIPmentation peaks were annotated with the R package ChIPseeker[84]. Promoters were defined as ATAC-seq peaks that overlap H3K27ac

peaks and are within 2 kb of an annotated transcription start site (TSS). Enhancers were defined as ATAC-seq peaks that overlap H3K27ac peaks and are 2 kb or more away from an annotated TSS. In heatmaps and metaplots depicting enhancers, ChIP-seq signal was centred on the enhancer ATAC peak for cell lines. For patient samples missing ATAC data, the ChIP-seq signal was centred on H3K27ac peaks. Enhancers were assigned to genes using the nearest annotated TSS.

Immunoprecipitation Mass Spectrometry. Data search was performed in a library-free search in DIA-NN[85] 1.8.1 with the database UPR UPR_Homo sapiens_9606_UP000005640_20200803.fasta. FDR (false discovery rate) was set to 0.01 and MBR (match between runs) was enabled. Mass spec intensities were normalized by MaxLFQ (generic label free technology) and transformed to log2. Imputation was performed in R by replacing missing values with randomly sampled values from a down-shifted normal distribution following methods described in[86]. Keratins and common contaminants identified in 95% of the CRAPome database[87] were excluded from the data. Comparisons between conditions (IgG and Menin IPs) were performed with moderated t-tests using the R package Genoppi[88] (https://github.com/lagelab/Genoppi) and corrected for multiple comparisons using False Discovery Rate with the R package fdrtools[89] Volcano plots were generated using ggplot2. Enrichment analyses were performed with a hypergeometric test from the Genoppi package using the CORUM database[50].

Micro-Capture-C. Analysis was performed using the Micro-Capture-C pipeline from the Davies lab (https://github.com/jojdavies/Micro-Capture-C). Peak calling was performed with deep-learning-based peak caller LanceOtron[90]. The peaks were filtered using a custom script from the Davies Lab based on size, width, and distance from the capture viewpoint. Unique junctions were counted at each peak site, then normalized using cis-unique ligation for the corresponding viewpoint as previously reported[61]. Peak junctions were compared between conditions using a Mann-Whitney U test corrected for multiple comparisons using R package fdrtools, and comparisons were visualized in R using ggplot2. MCC peaks were intersected with Menin ChIP-seq peaks. Pearson's chi-square test was used to test for independence between Menin peaks and differential MCC peaks.

References

1. Strahl, B.D. & Allis, C.D. The language of covalent histone modifications. *Nature* **403**, 41-45 (2000).

2. Dawson, M.A. & Kouzarides, T. Cancer epigenetics: from mechanism to therapy. *Cell* **150**, 12-27 (2012).

3. Bhagwat, A.S., Lu, B. & Vakoc, C.R. Enhancer dysfunction in leukemia. *Blood* **131**, 1795-1804 (2018).

4. Siklos, M. & Kubicek, S. Therapeutic targeting of chromatin: status and opportunities. *FEBS J* **289**, 1276-1301 (2022).

5. Cheng, Y. *et al.* Targeting epigenetic regulators for cancer therapy: mechanisms and advances in clinical trials. *Signal Transduct Target Ther* **4**, 62 (2019).

6. Mabe, N.W., Perry, J.A., Malone, C.F. & Stegmaier, K. Pharmacological targeting of the cancer epigenome. *Nat Cancer* **5**, 844-865 (2024).

7. Brown, M.R. & Soto-Feliciano, Y.M. Menin: from molecular insights to clinical impact. *Epigenomics* **17**, 489-505 (2025).

8. Balogh, K., Racz, K., Patocs, A. & Hunyady, L. Menin and its interacting proteins: elucidation of menin function. *Trends Endocrinol Metab* **17**, 357-364 (2006).

9. Matkar, S., Thiel, A. & Hua, X. Menin: a scaffold protein that controls gene expression and cell signaling. *Trends Biochem Sci* **38**, 394-402 (2013).

10. Balogh, K., Patocs, A., Hunyady, L. & Racz, K. Menin dynamics and functional insight: take your partners. *Mol Cell Endocrinol* **326**, 80-84 (2010).

11. Issa, G.C. *et al.* The menin inhibitor revumenib in KMT2A-rearranged or NPM1-mutant leukaemia. *Nature* **615**, 920-924 (2023).

12. Borkhardt, A. *et al.* Infant acute lymphoblastic leukemia - combined cytogenetic, immunophenotypical and molecular analysis of 77 cases. *Leukemia* **16**, 1685-1690 (2002).

13. Rice, S. & Roy, A. MLL-rearranged infant leukaemia: A 'thorn in the side' of a remarkable success story. *Biochim Biophys Acta Gene Regul Mech* **1863**, 194564 (2020).

14. Winters, A.C. & Bernt, K.M. MLL-Rearranged Leukemias-An Update on Science and Clinical Approaches. *Front Pediatr* **5**, 4 (2017).

15. Meyer, C. *et al.* The MLL recombinome of acute leukemias in 2017. *Leukemia* **32**, 273-284 (2018).

16. Takahashi, S. & Yokoyama, A. The molecular functions of common and atypical MLL fusion protein complexes. *Biochim Biophys Acta Gene Regul Mech* **1863**, 194548 (2020).

17. Basu, S., Nandy, A. & Biswas, D. Keeping RNA polymerase II on the run: Functions of MLL fusion partners in transcriptional regulation. *Biochim Biophys Acta Gene Regul Mech* **1863**, 194563 (2020).

18. Slany, R.K. MLL fusion proteins and transcriptional control. *Biochim Biophys Acta Gene Regul Mech* **1863**, 194503 (2020).

19. Yokoyama, A. *et al.* The menin tumor suppressor protein is an essential oncogenic cofactor for MLL-associated leukemogenesis. *Cell* **123**, 207-218 (2005).

20. Grembecka, J. *et al.* Menin-MLL inhibitors reverse oncogenic activity of MLL fusion proteins in leukemia. *Nat Chem Biol* **8**, 277-284 (2012).

21. Uckelmann, H.J. *et al.* Mutant NPM1 Directly Regulates Oncogenic Transcription in Acute Myeloid Leukemia. *Cancer Discov* **13**, 746-765 (2023).

22. Klossowski, S. *et al.* Menin inhibitor MI-3454 induces remission in MLL1-rearranged and NPM1-mutated models of leukemia. *J Clin Invest* **130**, 981-997 (2020).

23. Uckelmann, H.J. *et al.* Therapeutic targeting of preleukemia cells in a mouse model of NPM1 mutant acute myeloid leukemia. *Science* **367**, 586-590 (2020).

24. Wang, X.Q.D. *et al.* Mutant NPM1 Hijacks Transcriptional Hubs to Maintain Pathogenic Gene Programs in Acute Myeloid Leukemia. *Cancer Discov* **13**, 724-745 (2023).

25. Kuhn, M.W. *et al.* Targeting Chromatin Regulators Inhibits Leukemogenic Gene Expression in NPM1 Mutant Leukemia. *Cancer Discov* **6**, 1166-1181 (2016).

26. Rau, R. & Brown, P. Nucleophosmin (NPM1) mutations in adult and childhood acute myeloid leukaemia: towards definition of a new leukaemia entity. *Hematol Oncol* **27**, 171-181 (2009).

27. Ranieri, R. *et al.* Current status and future perspectives in targeted therapy of NPM1-mutated AML. *Leukemia* **36**, 2351-2367 (2022).

28. Bolli, N. *et al.* Born to be exported: COOH-terminal nuclear export signals of different strength ensure cytoplasmic accumulation of nucleophosmin leukemic mutants. *Cancer Res* **67**, 6230-6237 (2007).

29. Falini, B. *et al.* Both carboxy-terminus NES motif and mutated tryptophan(s) are crucial for aberrant nuclear export of nucleophosmin leukemic mutants in NPMc+ AML. *Blood* **107**, 4514-4523 (2006).

30. Falini, B. *et al.* Cytoplasmic nucleophosmin in acute myelogenous leukemia with a normal karyotype. *N Engl J Med* **352**, 254-266 (2005).

31. Alcalay, M. *et al.* Acute myeloid leukemia bearing cytoplasmic nucleophosmin (NPMc+ AML) shows a distinct gene expression profile characterized by up-regulation of genes involved in stem-cell maintenance. *Blood* **106**, 899-902 (2005).

32. Brunetti, L. *et al.* Mutant NPM1 Maintains the Leukemic State through HOX Expression. *Cancer Cell* **34**, 499-512 e499 (2018).

33. Krivtsov, A.V. *et al.* A Menin-MLL Inhibitor Induces Specific Chromatin Changes and Eradicates Disease in Models of MLL-Rearranged Leukemia. *Cancer Cell* **36**, 660-673 e611 (2019).

34. Kerry, J. *et al.* MLL-AF4 Spreading Identifies Binding Sites that Are Distinct from Super-Enhancers and that Govern Sensitivity to DOT1L Inhibition in Leukemia. *Cell Rep* **18**, 482-495 (2017).

35. Prange, K.H.M. *et al.* MLL-AF9 and MLL-AF4 oncofusion proteins bind a distinct enhancer repertoire and target the RUNX1 program in 11q23 acute myeloid leukemia. *Oncogene* **36**, 3346-3356 (2017).

36. Godfrey, L. *et al.* DOT1L inhibition reveals a distinct subset of enhancers dependent on H3K79 methylation. *Nature communications* **10**, 2803 (2019).

37. Crump, N.T. *et al.* MLL-AF4 cooperates with PAF1 and FACT to drive high-density enhancer interactions in leukemia. *Nature communications* **14**, 5208 (2023).

38. Smith, A.L. *et al.* Enhancer heterogeneity in acute lymphoblastic leukemia drives differential gene expression in patients. *Blood* **146**, 2073-2087 (2025).

39. Panigrahi, A. & O'Malley, B.W. Mechanisms of enhancer action: the known and the unknown. *Genome Biol* **22**, 108 (2021).

40. Pan, F. *et al.* Enhancer remodeling drives MLL oncogene-dependent transcriptional dysregulation in leukemia stem cells. *Blood Adv* **7**, 2504-2519 (2023).

41. Dreijerink, K.M.A. *et al.* Enhancer-Mediated Oncogenic Function of the Menin Tumor Suppressor in Breast Cancer. *Cell Rep* **18**, 2359-2372 (2017).

42. Sun, J., Yu, W. & Zhang, X. MENIN inhibitor-based therapy in acute leukemia: latest updates from the 2024 ASH annual meeting. *Exp Hematol Oncol* **14**, 78 (2025).

43. Candoni, A. & Coppola, G. A 2024 Update on Menin Inhibitors. A New Class of Target Agents against KMT2A-Rearranged and NPM1-Mutated Acute Myeloid Leukemia. *Hematol Rep* **16**, 244-254 (2024).

44. Freire, P.R., Cutler, J.A. & Armstrong, S.A. Therapeutic Targeting of the Menin–KMT2A Interaction. *Annual Review Cancer Biology.* **8**, 291-307 (2024).

45. Schmidl, C., Rendeiro, A.F., Sheffield, N.C. & Bock, C. ChIPmentation: fast, robust, low-input ChIP-seq for histones and transcription factors. *Nat Methods* **12**, 963-965 (2015).

46. Gustafsson, C., De Paepe, A., Schmidl, C. & Mansson, R. High-throughput ChIPmentation: freely scalable, single day ChIPseq data generation from very low cell-numbers. *BMC Genomics* **20**, 59 (2019).

47. Ciaurro, V. *et al.* Menin inhibitor DS-1594b drives differentiation and induces synergistic lethality in combination with venetoclax in acute myeloid leukemia cells with rearranged mixed-lineage leukemia and mutated nucleophosmin-1. *Haematologica* (2025).

48. Okuda, H. *et al.* MLL fusion proteins link transcriptional coactivators to previously active CpG-rich promoters. *Nucleic Acids Res* **42**, 4241-4256 (2014).

49. Milne, T.A. *et al.* MLL associates specifically with a subset of transcriptionally active target genes. *Proc Natl Acad Sci U S A* **102**, 14765-14770 (2005).

50. Tsitsiridis, G. *et al.* CORUM: the comprehensive resource of mammalian protein complexes-2022. *Nucleic Acids Res* **51**, D539-D545 (2023).

51. Meyers, R.M. *et al.* Computational correction of copy number effect improves specificity of CRISPR-Cas9 essentiality screens in cancer cells. *Nat Genet* **49**, 1779-1784 (2017).

52. Mueller, D. *et al.* A role for the MLL fusion partner ENL in transcriptional elongation and chromatin modification. *Blood* **110**, 4445-4454 (2007).

53. Orphanides, G., LeRoy, G., Chang, C.H., Luse, D.S. & Reinberg, D. FACT, a factor that facilitates transcript elongation through nucleosomes. *Cell* **92**, 105-116 (1998).

54. Kim, J., Guermah, M. & Roeder, R.G. The human PAF1 complex acts in chromatin transcription elongation both independently and cooperatively with SII/TFIIS. *Cell* **140**, 491-503 (2010).

55. Raisner, R. *et al.* Enhancer Activity Requires CBP/P300 Bromodomain-Dependent Histone H3K27 Acetylation. *Cell Rep* **24**, 1722-1729 (2018).

56. Hogg, S.J. *et al.* Targeting histone acetylation dynamics and oncogenic transcription by catalytic P300/CBP inhibition. *Mol Cell* **81**, 2183-2200 e2113 (2021).

57. Janssens, D.H. *et al.* Automated CUT&Tag profiling of chromatin heterogeneity in mixed-lineage leukemia. *Nat Genet* **53**, 1586-1596 (2021).

58. Chen, H. *et al.* Dynamic interplay between enhancer-promoter topology and gene activity. *Nat Genet* **50**, 1296-1303 (2018).

59. Brown, J.M. *et al.* A tissue-specific self-interacting chromatin domain forms independently of enhancer-promoter interactions. *Nature communications* **9**, 3849 (2018).

60. Nollmann, M., Bennabi, I., Gotz, M. & Gregor, T. The Impact of Space and Time on the Functional Output of the Genome. *Cold Spring Harb Perspect Biol* **14** (2022).

61. Hua, P. *et al.* Defining genome architecture at base-pair resolution. *Nature* **595**, 125-129 (2021).

62. Yokoyama, A., Lin, M., Naresh, A., Kitabayashi, I. & Cleary, M.L. A higher-order complex containing AF4 and ENL family proteins with P-TEFb facilitates oncogenic and physiologic MLL-dependent transcription. *Cancer Cell* **17**, 198-212 (2010).

63. Krivtsov, A.V. *et al.* Transformation from committed progenitor to leukaemia stem cell initiated by MLL-AF9. *Nature* **442**, 818-822 (2006).

64. Adriaanse, F.R.S. *et al.* Distinct Responses to Menin Inhibition and Synergy with DOT1L Inhibition in KMT2A-Rearranged Acute Lymphoblastic and Myeloid Leukemia. *Int J Mol Sci* **25** (2024).

65. Perner, F., Gadrey, J.Y., Armstrong, S.A. & Kuhn, M.W.M. Targeting the Menin-KMT2A interaction in leukemia: Lessons learned and future directions. *Int J Cancer* **158**, 342-356 (2026).

66. Xu, H. *et al.* NUP98 Fusion Proteins Interact with the NSL and MLL1 Complexes to Drive Leukemogenesis. *Cancer Cell* **30**, 863-878 (2016).

67. Barajas, J.M. *et al.* Acute myeloid leukemias with UBTF tandem duplications are sensitive to menin inhibitors. *Blood* **143**, 619-630 (2024).

68. Olsen, S.N. *et al.* Combined inhibition of KAT6A/B and Menin reverses estrogen receptor-driven gene expression programs in breast cancer. *Cell Rep Med* **6**, 102192 (2025).

69. Hemming, M.L. *et al.* MOZ and Menin-MLL Complexes Are Complementary Regulators of Chromatin Association and Transcriptional Output in Gastrointestinal Stromal Tumor. *Cancer Discov* **12**, 1804-1823 (2022).

70. Perner, F. *et al.* MEN1 mutations mediate clinical resistance to menin inhibition. *Nature* **615**, 913-919 (2023).

71. Ritz, C., Baty, F., Streibig, J.C. & Gerhard, D. Dose-Response Analysis Using R. *PLoS One* **10**, e0146021 (2015).

72. Buenrostro, J.D., Wu, B., Chang, H.Y. & Greenleaf, W.J. ATAC-seq: A Method for Assaying Chromatin Accessibility Genome-Wide. *Curr Protoc Mol Biol* **109**, 21 29 21-21 29 29 (2015).

73. Schwalb, B. *et al.* TT-seq maps the human transient transcriptome. *Science* **352**, 1225-1228 (2016).

74. Hamley, J.C., Li, H., Denny, N., Downes, D. & Davies, J.O.J. Determining chromatin architecture with Micro Capture-C. *Nat Protoc* **18**, 1687-1711 (2023).

75. Langmead, B. & Salzberg, S.L. Fast gapped-read alignment with Bowtie 2. *Nat Methods* **9**, 357-359 (2012).

76. Ramirez, F., Dundar, F., Diehl, S., Gruning, B.A. & Manke, T. deepTools: a flexible platform for exploring deep-sequencing data. *Nucleic Acids Res* **42**, W187-191 (2014).

77. Heinz, S. *et al.* Simple combinations of lineage-determining transcription factors prime cis-regulatory elements required for macrophage and B cell identities. *Mol Cell* **38**, 576-589 (2010).

78. Stark, R. & Brown, G. DiffBind: differential binding analysis of ChIP-Seq peak data. . *Bioconductor* (2011).

79. Gu, Z., Eils, R. & Schlesner, M. Complex heatmaps reveal patterns and correlations in multidimensional genomic data. *Bioinformatics* **32**, 2847-2849 (2016).

80. Dobin, A. *et al.* STAR: ultrafast universal RNA-seq aligner. *Bioinformatics* **29**, 15-21 (2013).

81. Liao, Y., Smyth, G.K. & Shi, W. featureCounts: an efficient general purpose program for assigning sequence reads to genomic features. *Bioinformatics* **30**, 923-930 (2014).

82. Robinson, M.D., McCarthy, D.J. & Smyth, G.K. edgeR: a Bioconductor package for differential expression analysis of digital gene expression data. *Bioinformatics* **26**, 139-140 (2010).

83. Patil, I. Visualizations with statistical details: the 'ggstatsplot' approach. *J. Open Source Softw.* **6**, 3167 (2021).

84. Yu, G., Wang, L.G. & He, Q.Y. ChIPseeker: an R/Bioconductor package for ChIP peak annotation, comparison and visualization. *Bioinformatics* **31**, 2382-2383 (2015).

85. Demichev, V., Messner, C.B., Vernardis, S.I., Lilley, K.S. & Ralser, M. DIA-NN: neural networks and interference correction enable deep proteome coverage in high throughput. *Nat Methods* **17**, 41-44 (2020).

86. Tyanova, S. *et al.* The Perseus computational platform for comprehensive analysis of (prote)omics data. *Nat Methods* **13**, 731-740 (2016).

87. Mellacheruvu, D. *et al.* The CRAPome: a contaminant repository for affinity purification-mass spectrometry data. *Nat Methods* **10**, 730-736 (2013).

88. Pintacuda, G. *et al.* Genoppi is an open-source software for robust and standardized integration of proteomic and genetic data. *Nature communications* **12**, 2580 (2021).

89. Strimmer, K. fdrtool: a versatile R package for estimating local and tail area-based false discovery rates. *Bioinformatics* **24**, 1461-1462 (2008).

90. Hentges, L.D. *et al.* LanceOtron: a deep learning peak caller for genome sequencing experiments. *Bioinformatics* **38**, 4255-4263 (2022).

Fig. 1: Differential effects of Menin inhibition on transcription in distinct leukemia subtypes.

a, Volcano plots of transient transcriptome RNA-seq after 24 h of treatment with DMSO or 250 nM Menin inhibitor VTP50469. **b**, Mean Menin binding (RRPM = reference normalised ChIP-seq reads per million) in SEM, RCH-ACV, and OCI-AML3 cells at promoters of differentially expressed genes in control (DMSO) or Menin inhibitor treatment (MENi). **c**, Proportion of differentially expressed genes (n.s. = not significant) following MENi with Menin binding at the promoter (± 2 kb around the TSS). Reported *p*-values are from a Pearson chi-square test. **d**, Intersections of all Menin-bound genes in the cell line panel. **e**, Intersections of downregulated Menin target genes in the cell line panel. **f**, Examples of Menin ChIP-seq in cell lines (SEM, RCH-ACV, and OCI-AML3) and ChIPmentation in primary patient samples (NPM1c-AML, iALL28349, and iALL863388) at down-regulated genes after 24 h MENi in the indicated cell lines.

Fig. 2: Gene expression correlates with MLL or NPM1c promoter binding at a subset of genes.

a, Gene expression changes at two time points of MENi in SEM and OCI-AML3 cells distinguish early and delayed transcription effects. The color of the flows corresponds to the gene expression status at the longest treatment time point (24 h in SEM and 72 h in OCI-AML3). Darker flows represent Menin-bound genes. **b**, Clustered heatmaps of differential (p.adj <0.05) MLL-AF4 peaks in SEM cells **(left)** or NPM1c peaks in OCI-AML3 cells **(right)** at two timepoints of MENi (n=2). Heatmaps of Menin and wild-type MLL binding (in OCI-AML3 cells only) are shown centred on the same sites, spanning a 2 kb region. Peaks are annotated as promoter if within 2 kb of a TSS or "other" if more than 2 kb away from a TSS. **c**, Examples of Menin, MLL/MLL-AF4, and NPM1c binding at differential peaks in SEM cells **(left)** and OCI-AML3 cells **(right)**. **d**, Scatter plots correlating changes in gene expression and changes in MLL/MLL-AF4 or NPM1c binding following MENi (250nM). Genes are colored if they display a significant alteration (p-adj < 0.05) in both expression and MLL-AF4/NPM1c binding, whereas non-significant genes are shown in grey.

Fig. 3: Menin associates with transcriptional regulators in leukemia cells.

a, UpSet plot representing significantly enriched proteins (FDR < 0.01 compared to IgG controls) co-immunoprecipitated with Menin in SEM, OCI-AML3, and RCH-ACV cells. **b**, Heatmap of statistically enriched Menin interactors in SEM, RCH-ACV and OCI-AML3 cells. **c**, Global enrichment of select complexes involved in transcription in Menin co-immunoprecipitations. **d**, Correlation between the gene effect scores reported in DepMap for

SEM and OCI-AML3 CRISPR screens. Proteins within complexes specifically enriched in SEM cells are colored. Genes with an effect score of < -1 in both cell lines are labelled.

Fig. 4: Menin binding is associated with intragenic enhancer activity.

a, Heatmaps of Menin ChIP-seq at promoters and enhancers in SEM, RCH-ACV, and OCI-AML3 cells. Regions are sorted by H3K27ac signal and centered on ATAC peaks. **b**, Heatmaps of Menin ChIPmentation at promoters and enhancers, centred on H3K27ac peaks, in primary samples from two infant MLL-AF4 ALL patients (iALL28349, iALL863388) and one adult NPM1-mutated AML patient. **c**, Association between Menin binding at intragenic enhancers and differential gene expression from the nearest TSS following 24 h of MENi. *p*-values are reported from a Pearson chi-square test. **d**, Mean Menin, MLL/MLL-AF4, and H3K27ac at intragenic enhancers annotated to differentially expressed genes by nearest TSS after 24 h of MENi in SEM and OCI-AML3 cells.

Fig. 5: Menin binds promoter contact sites in MLL-AF4 cells.

a, Proportion of MCC peaks (enhancer-promoter contacts) bound by Menin in SEM and OCI-AML3 cells. **b**, Annotation of MCC peaks with or without Menin binding in SEM and OCI-AML3 cells. **c**, Mean Menin, MLL/MLL-AF4, H3K27ac, and NPM1c signal at MCC peaks in SEM cells **(top)** and OCI-AML3 cells **(bottom)**, clustered by Menin ChIP-seq signal (k-means = 3). **d**, Visualization of MCC and ChIP-seq signal at the *ARID1B* locus **(left)** and *FLT3* locus **(right)** in SEM and OCI-AML3 cells. The subtraction track shows the difference in MCC signal between the DMSO and MENi (250 nM, 24 h) conditions. MCC peaks of interest are highlighted in pink and annotated with numbers.

Fig. 6: MENi disrupts enhancer-promoter contacts in MLL-AF4 cells but not NPM1c cells.

a, Changes in mean ligation junction counts at MCC peaks in SEM **(left)** and OCI-AML3 **(right)** cells treated with MENi (250 nM, 24 h), categorised by Menin binding. Colored data points represent significantly altered contacts (Mann-Whitney U q-value < 0.05). *p*-values comparing bound and unbound sites are reported from a Wilcoxon test. **b**, Genomic annotation of decreased MCC peaks bound by Menin in SEM cells. **c**, Scatter plots showing the change in interaction frequency correlated with the change in H3K27ac, Menin or MLL/MLL-AF4 enrichment after 24 h of MENi (250 nM) in SEM cells. Colored data points are sites with a significant (MWU FDR q-value < 0.05) change in interaction. A linear fit is shown specifically for sites of decreased interaction. **d**, Quantification of Menin ChIP-seq signal at differential MCC peaks in SEM cells. **e**, Association between gene expression and enhancer-promoter interaction frequency following MENi (250 nM, 24 h) in SEM cells. For each gene with multiple

MCC peaks, the most statistically significant promoter interaction is presented. **f**, Genes with a significantly decreased enhancer-promoter contact and decreased expression after 24 h MENi (250 nM).

Fig. 7: Model of Menin activity in MLL-AF4 and NPM1-mutant leukemia.

MLL-AF4 uniquely co-opts Menin to associate more strongly with transcription co-activators and stabilize enhancer-promoter proximity to activate genes. MENi triggers rapid transcriptional changes in the context of MLL-AF4 ALL and delayed gene expression changes in NPM1-mutant AML.

Figure 1

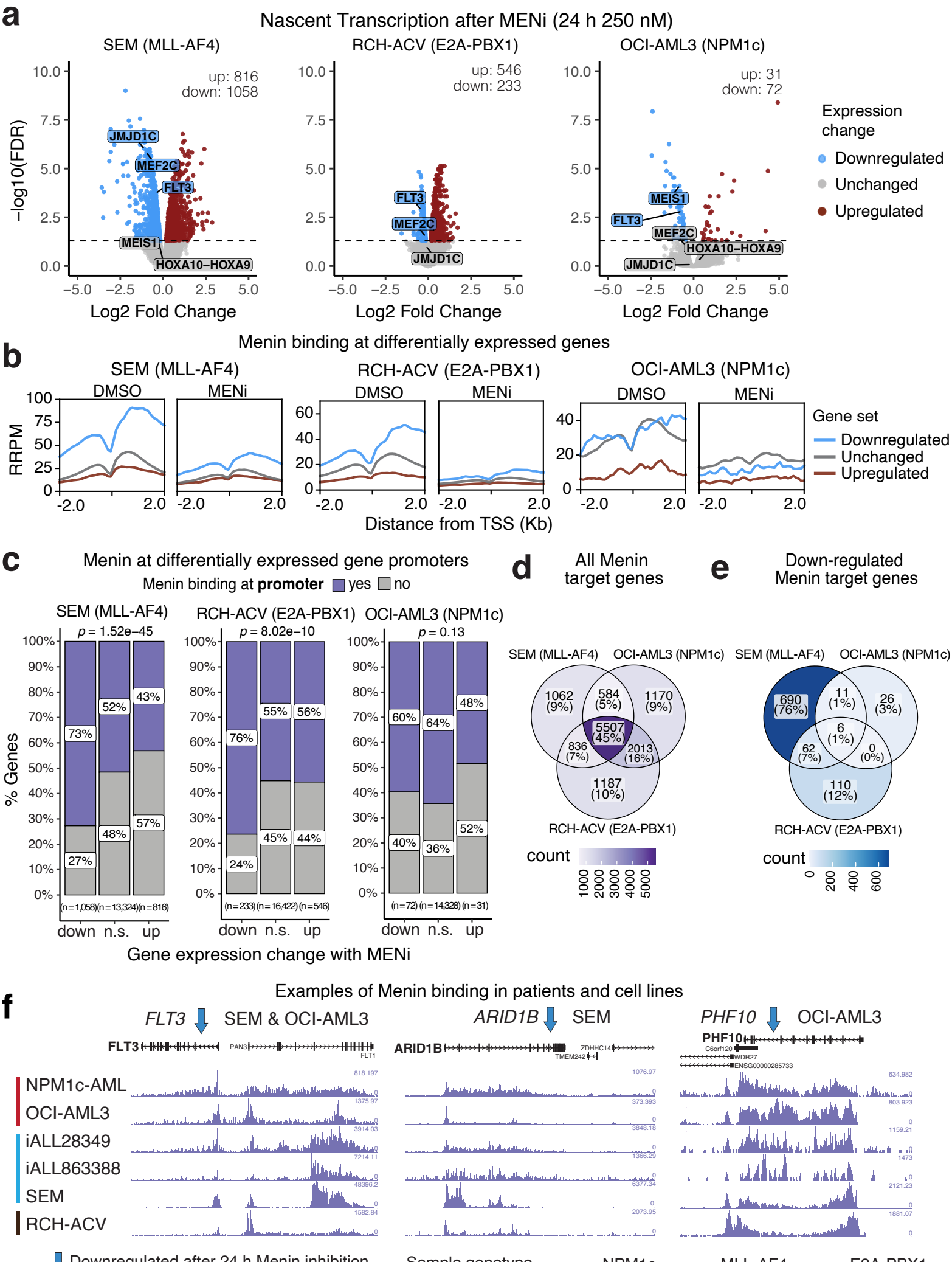

Fig. 1: Differential effects of Menin inhibition on transcription in distinct leukemia subtypes.

a, Volcano plots of transient transcriptome RNA-seq after 24 h of treatment with DMSO or 250 nM Menin inhibitor VTP50469. **b**, Mean Menin binding (RRPM = reference normalised ChIP-seq reads per million) in SEM, RCH-ACV, and OCI-AML3 cells at promoters of differentially expressed genes in control (DMSO) or Menin inhibitor treatment (MENi). **c**, Proportion of differentially expressed genes (n.s. = not significant) following MENi with Menin binding at the promoter (± 2 kb around the TSS). Reported *p*-values are from a Pearson chi-square test. **d**, Intersections of all Menin-bound genes in the cell line panel. **e**, Intersections of downregulated Menin target genes in the cell line panel. **f**, Examples of Menin ChIP-seq in cell lines (SEM, RCH-ACV, and OCI-AML3) and ChIPmentation in primary patient samples (NPM1c-AML, iALL28349, and iALL863388) at down-regulated genes after 24 h MENi in the indicated cell lines.

Figure 2

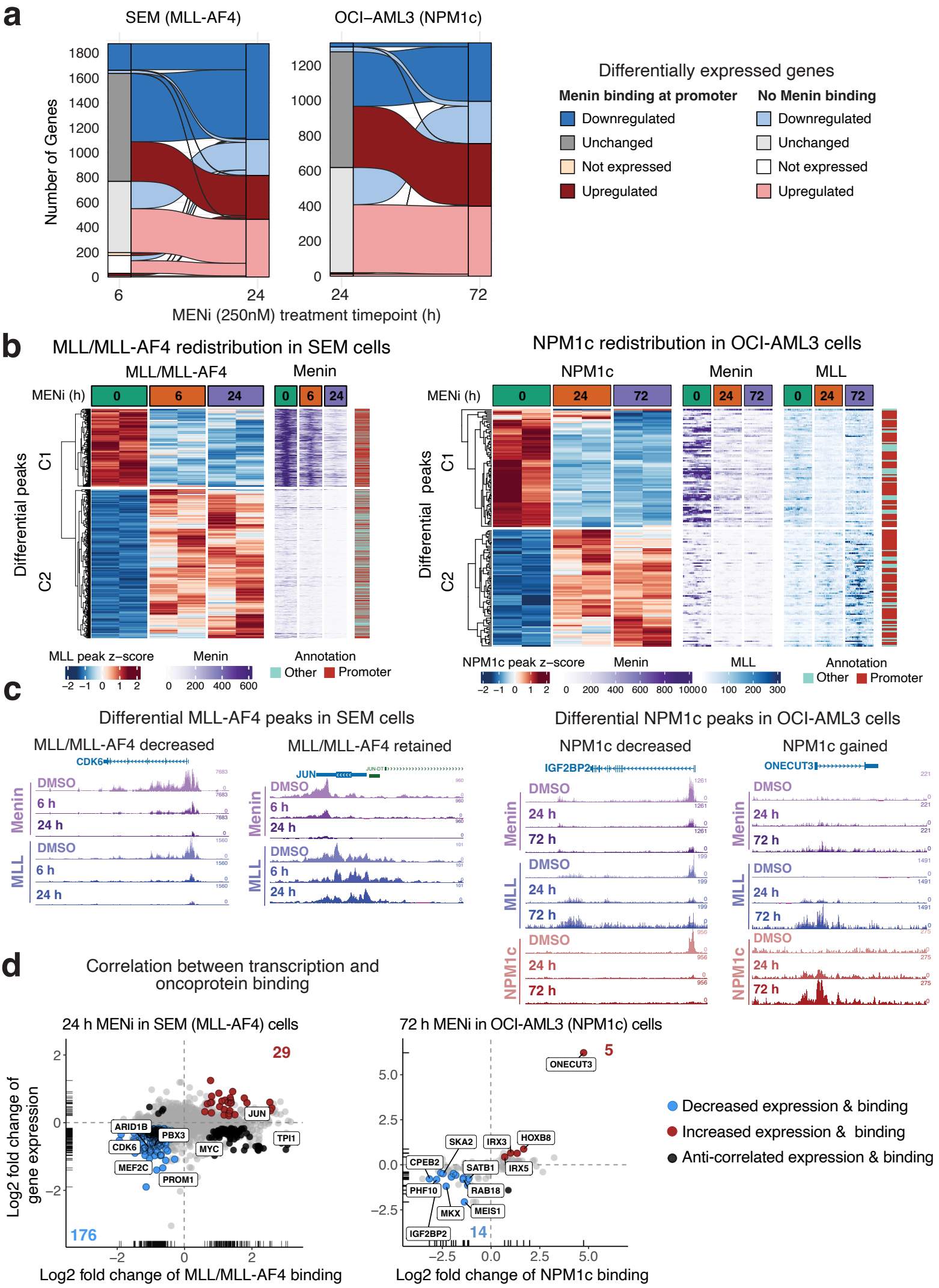

Fig. 2: Gene expression correlates with MLL or NPM1c promoter binding at a subset of genes.

a, Gene expression changes at two time points of MENi in SEM and OCI-AML3 cells distinguish early and delayed transcription effects. The color of the flows corresponds to the gene expression status at the longest treatment time point (24 h in SEM and 72 h in OCI-AML3). Darker flows represent Menin-bound genes. **b**, Clustered heatmaps of differential (p.adj <0.05) MLL-AF4 peaks in SEM cells **(left)** or NPM1c peaks in OCI-AML3 cells **(right)** at two timepoints of MENi (n=2). Heatmaps of Menin and wild-type MLL binding (in OCI-AML3 cells only) are shown centred on the same sites, spanning a 2 kb region. Peaks are annotated as promoter if within 2 kb of a TSS or "other" if more than 2 kb away from a TSS. **c**, Examples of Menin, MLL/MLL-AF4, and NPM1c binding at differential peaks in SEM cells **(left)** and OCI-AML3 cells **(right)**. **d**, Scatter plots correlating changes in gene expression and changes in MLL/MLL-AF4 or NPM1c binding following MENi (250nM). Genes are colored if they display a significant alteration (p-adj < 0.05) in both expression and MLL-AF4/NPM1c binding, whereas non-significant genes are shown in grey.

Figure 3

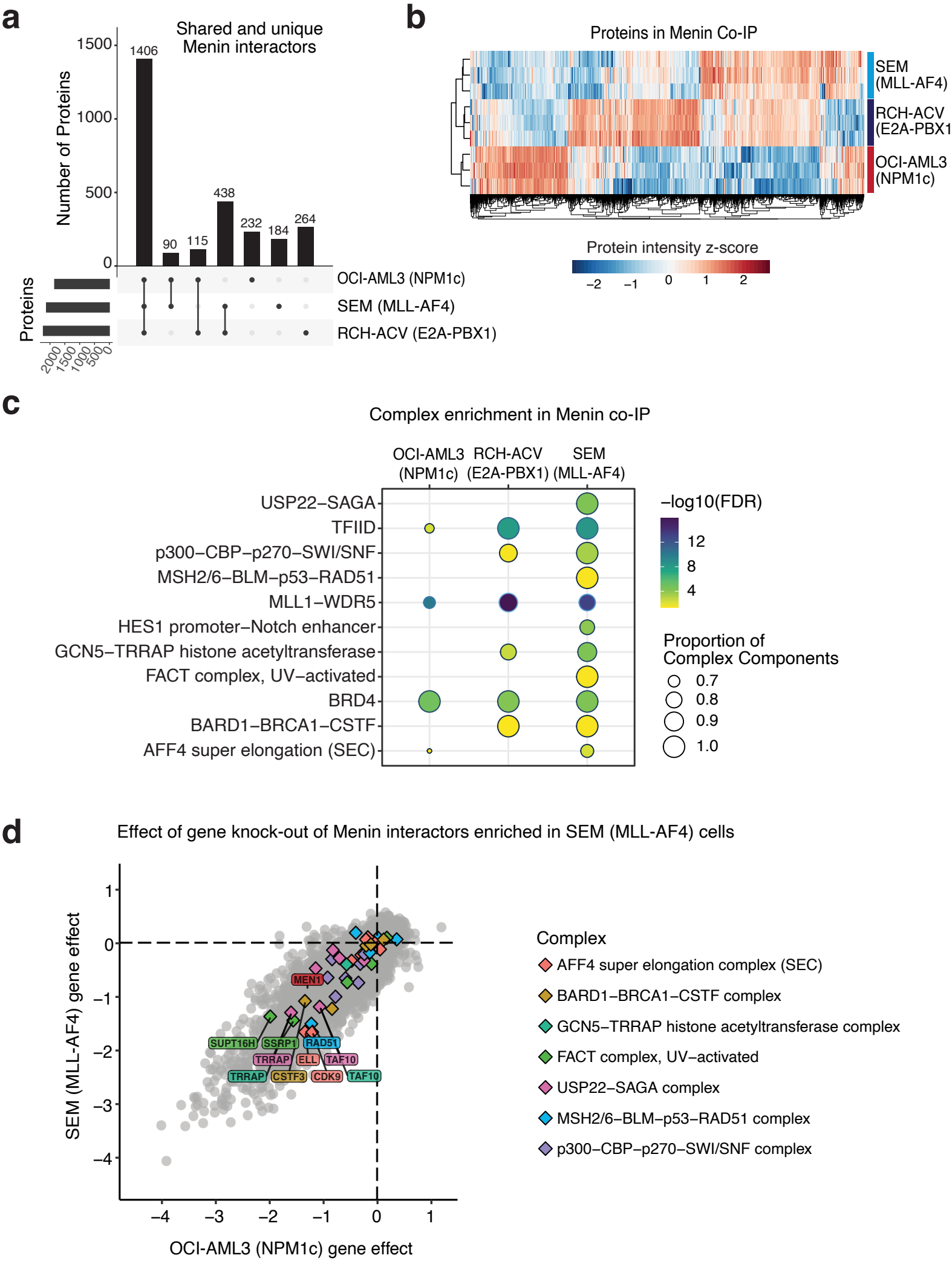

Fig. 3: Menin associates with transcriptional regulators in leukemia cells.

a, UpSet plot representing significantly enriched proteins (FDR < 0.01 compared to IgG controls) co-immunoprecipitated with Menin in SEM, OCI-AML3, and RCH-ACV cells. **b**, Heatmap of statistically enriched Menin interactors in SEM, RCH-ACV and OCI-AML3 cells. **c**, Global enrichment of select complexes involved in transcription in Menin co-immunoprecipitations. **d**, Correlation between the gene effect scores reported in DepMap for SEM and OCI-AML3 CRISPR screens. Proteins within complexes specifically enriched in SEM cells are colored. Genes with an effect score of < -1 in both cell lines are labelled.

Figure 4

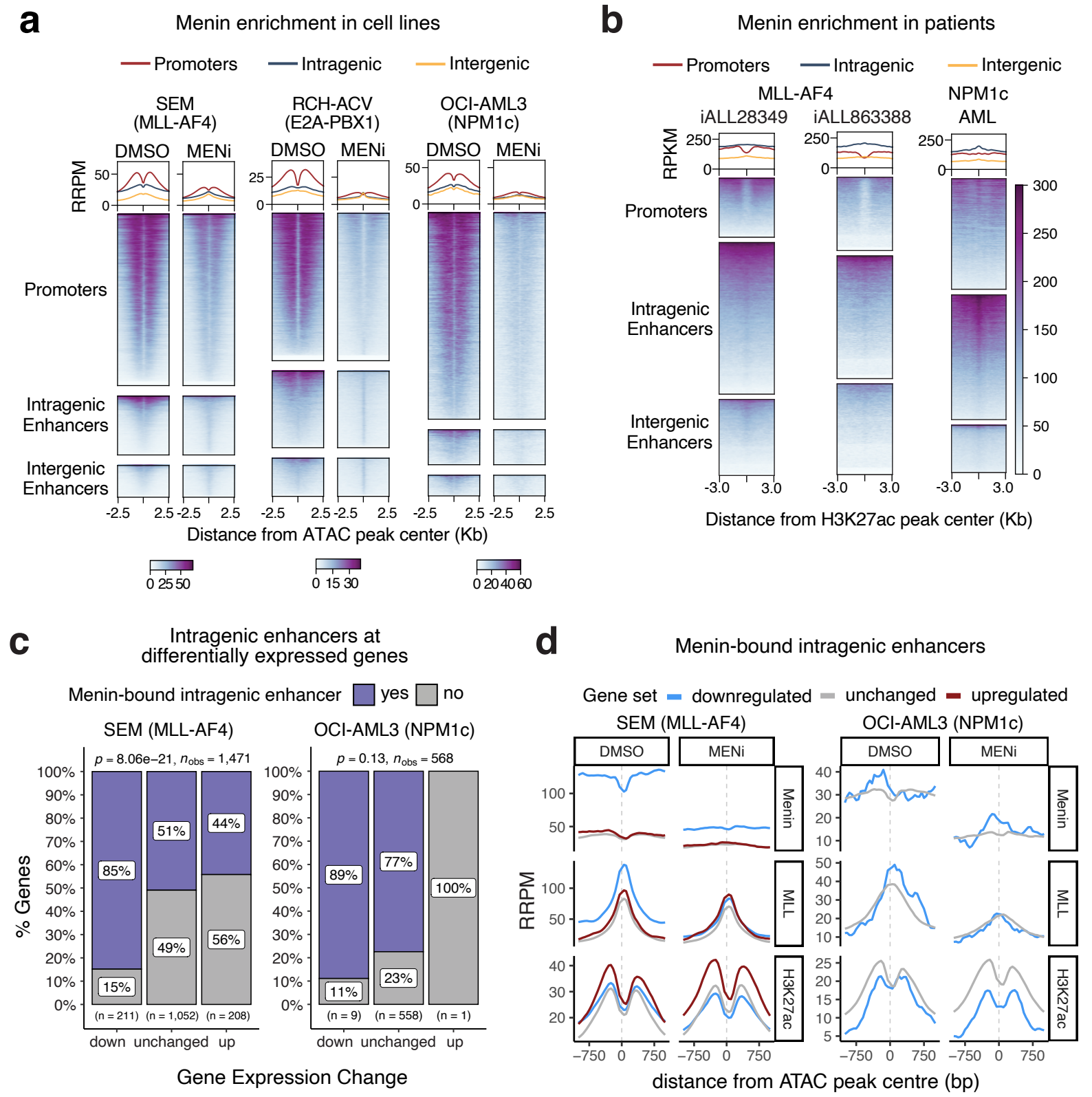

Fig. 4: Menin binding is associated with intragenic enhancer activity.

a, Heatmaps of Menin ChIP-seq at promoters and enhancers in SEM, RCH-ACV, and OCI-AML3 cells. Regions are sorted by H3K27ac signal and centered on ATAC peaks. **b**, Heatmaps of Menin ChIPmentation at promoters and enhancers, centred on H3K27ac peaks, in primary samples from two infant MLL-AF4 ALL patients (iALL28349, iALL863388) and one adult NPM1-mutated AML patient. **c**, Association between Menin binding at intragenic enhancers and differential gene expression from the nearest TSS following 24 h of MENi. *p*-values are reported from a Pearson chi-square test. **d**, Mean Menin, MLL/MLL-AF4, and H3K27ac at intragenic enhancers annotated to differentially expressed genes by nearest TSS after 24 h of MENi in SEM and OCI-AML3 cells.

Figure 5

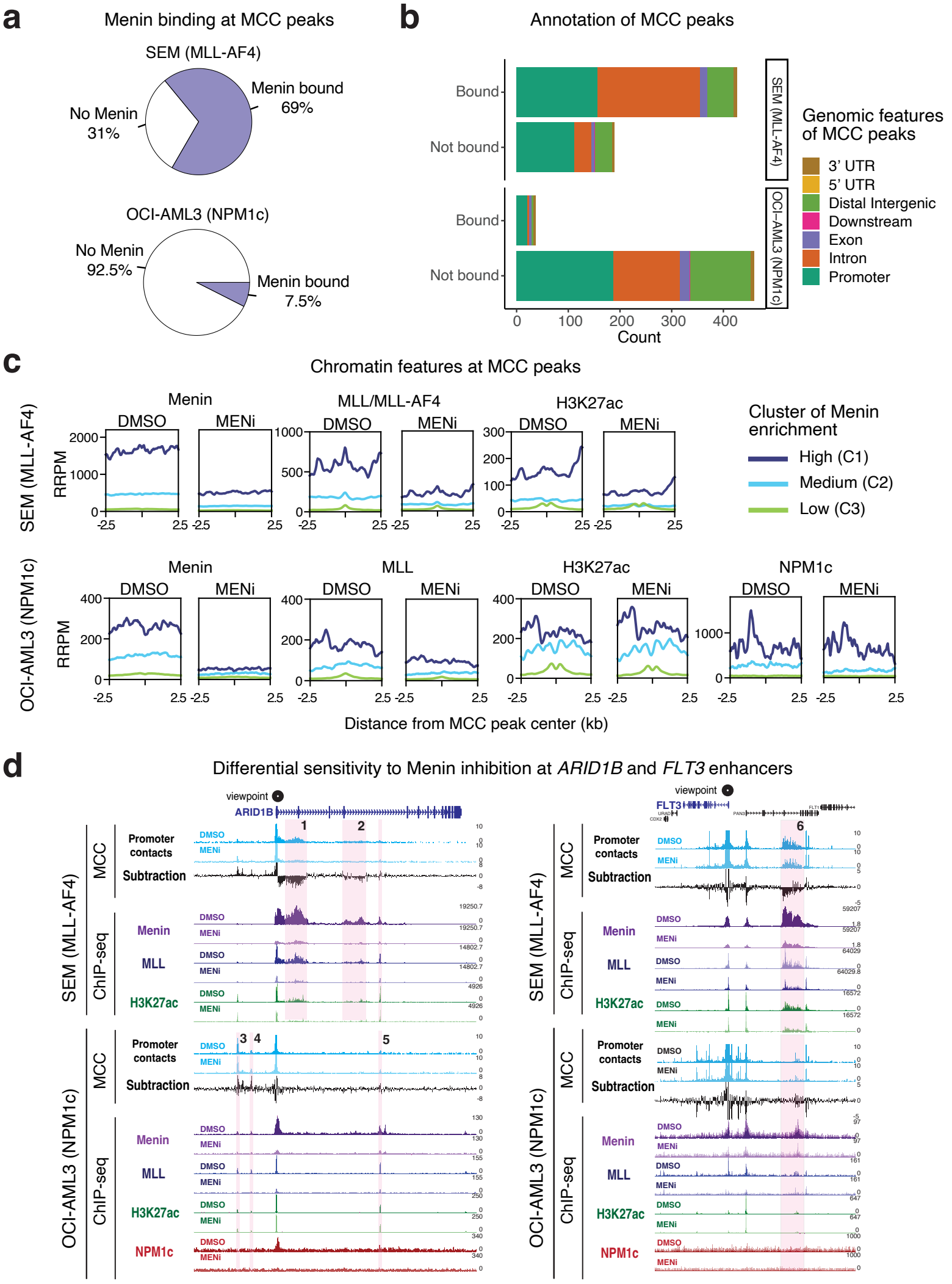

Fig. 5: Menin binds promoter contact sites in MLL-AF4 cells.

a, Proportion of MCC peaks (enhancer-promoter contacts) bound by Menin in SEM and OCI-AML3 cells. **b**, Annotation of MCC peaks with or without Menin binding in SEM and OCI-AML3 cells. **c**, Mean Menin, MLL/MLL-AF4, H3K27ac, and NPM1c signal at MCC peaks in SEM cells **(top)** and OCI-AML3 cells **(bottom)**, clustered by Menin ChIP-seq signal (k-means = 3). **d**, Visualization of MCC and ChIP-seq signal at the *ARID1B* locus **(left)** and *FLT3* locus **(right)** in SEM and OCI-AML3 cells. The subtraction track shows the difference in MCC signal between the DMSO and MENi (250 nM, 24 h) conditions. MCC peaks of interest are highlighted in pink and annotated with numbers.

Figure 6

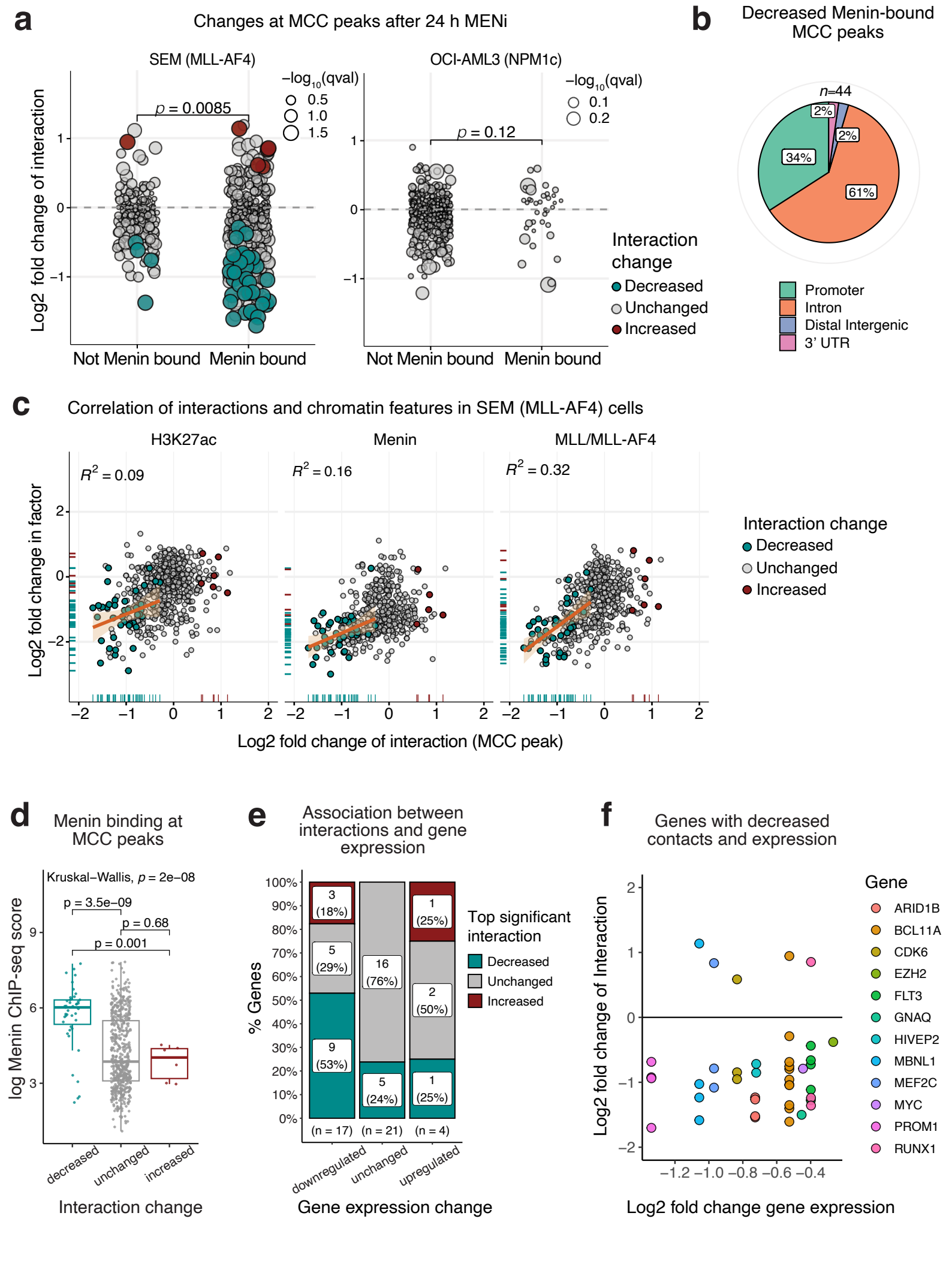

Fig. 6: MENi disrupts enhancer-promoter contacts in MLL-AF4 cells but not NPM1c cells.

a, Changes in mean ligation junction counts at MCC peaks in SEM **(left)** and OCI-AML3 **(right)** cells treated with MENi (250 nM, 24 h), categorised by Menin binding. Colored data points represent significantly altered contacts (Mann-Whitney U q-value < 0.05). *p*-values comparing bound and unbound sites are reported from a Wilcoxon test. **b**, Genomic annotation of decreased MCC peaks bound by Menin in SEM cells. **c**, Scatter plots showing the change in interaction frequency correlated with the change in H3K27ac, Menin or MLL/MLL-AF4 enrichment after 24 h of MENi (250 nM) in SEM cells. Colored data points are sites with a significant (MWU FDR q-value < 0.05) change in interaction. A linear fit is shown specifically for sites of decreased interaction. **d**, Quantification of Menin ChIP-seq signal at differential MCC peaks in SEM cells. **e**, Association between gene expression and enhancer-promoter interaction frequency following MENi (250 nM, 24 h) in SEM cells. For each gene with multiple MCC peaks, the most statistically significant promoter interaction is presented. **f**, Genes with a significantly decreased enhancer-promoter contact and decreased expression after 24 h MENi (250 nM).

Figure 7

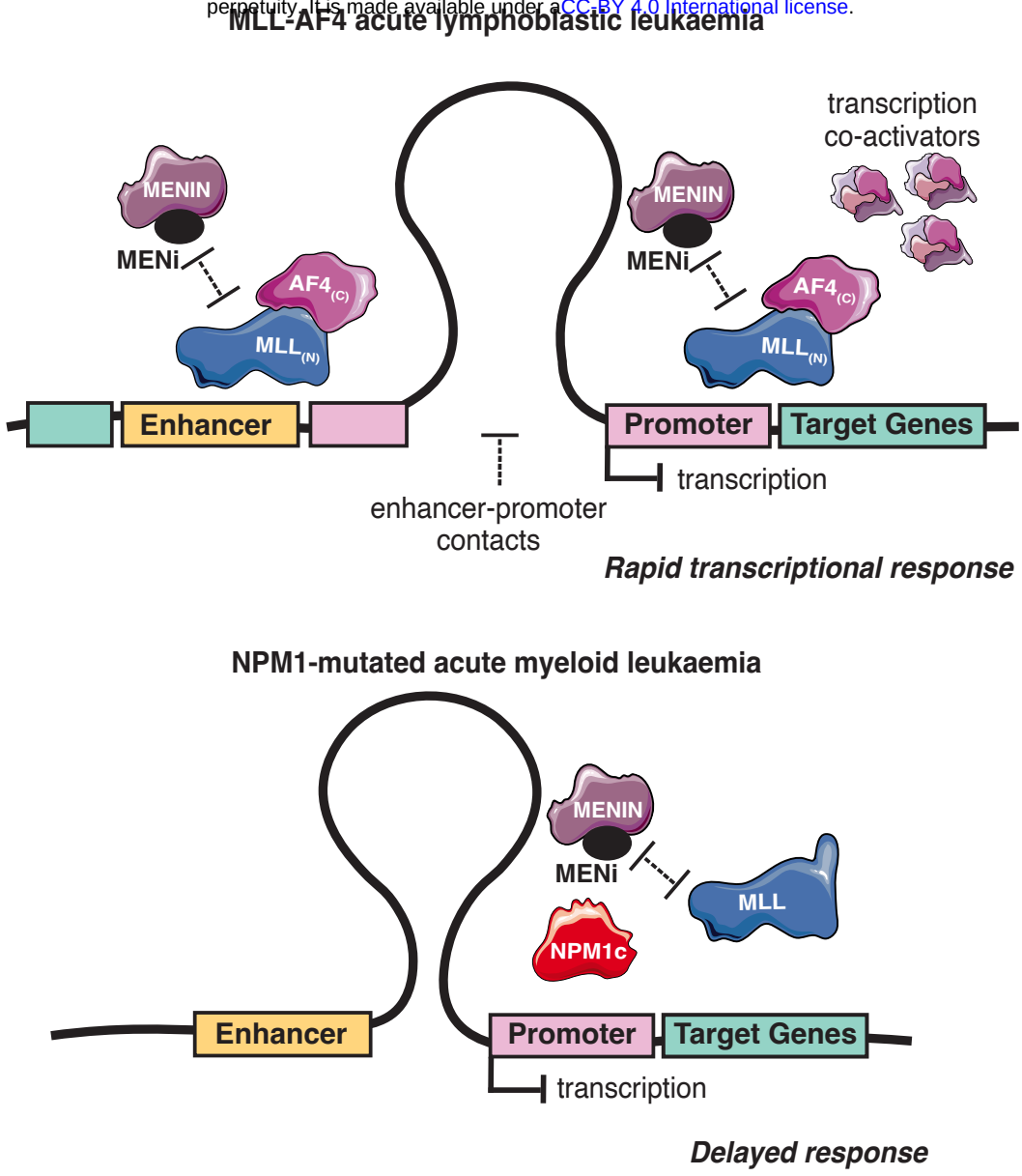

Fig. 7: Model of Menin activity in MLL-AF4 and NPM1-mutant leukemia.

MLL-AF4 uniquely co-opts Menin to associate more strongly with transcription co-activators and stabilize enhancer-promoter proximity to activate genes. MENi triggers rapid transcriptional changes in the context of MLL-AF4 ALL and delayed gene expression changes in NPM1-mutant AML.

Extended Data Figure 1

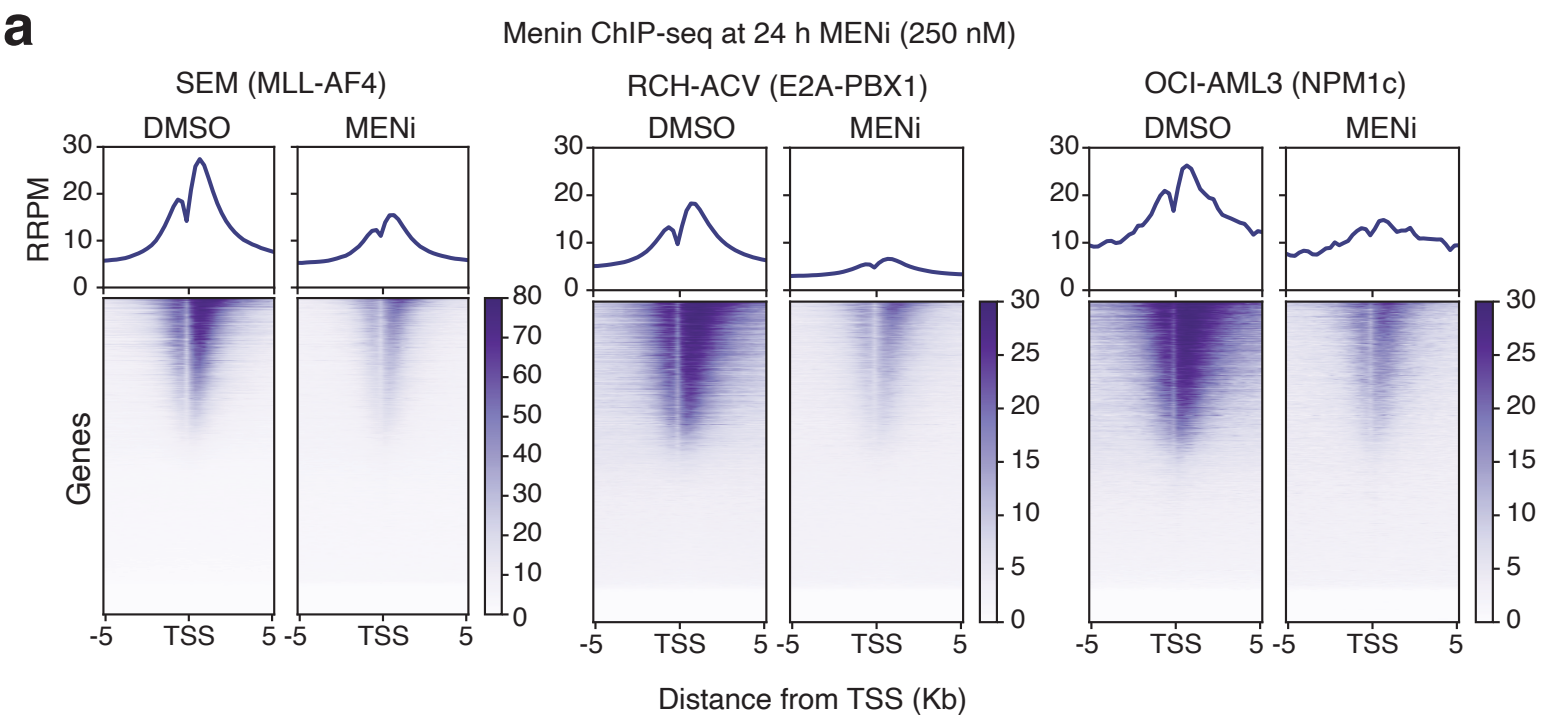

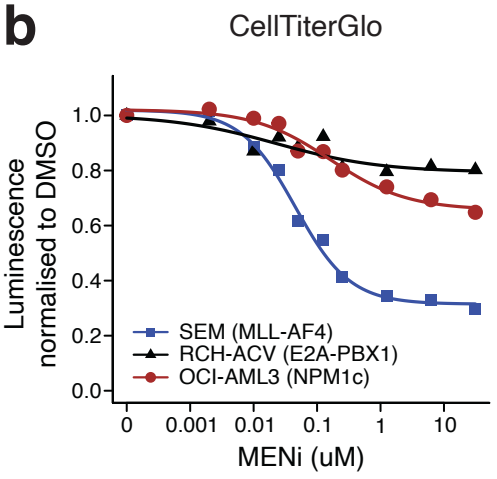

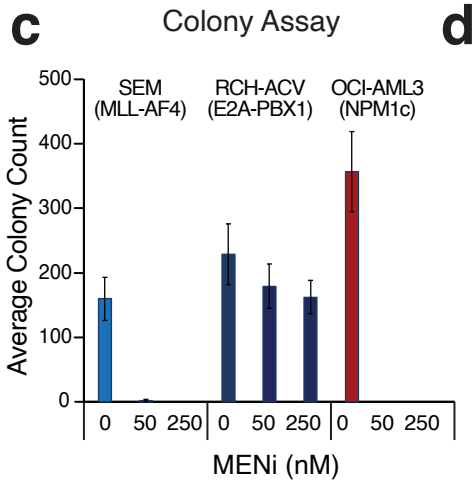

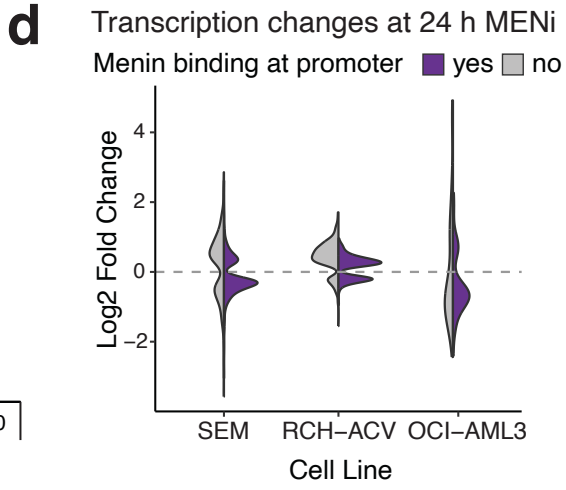

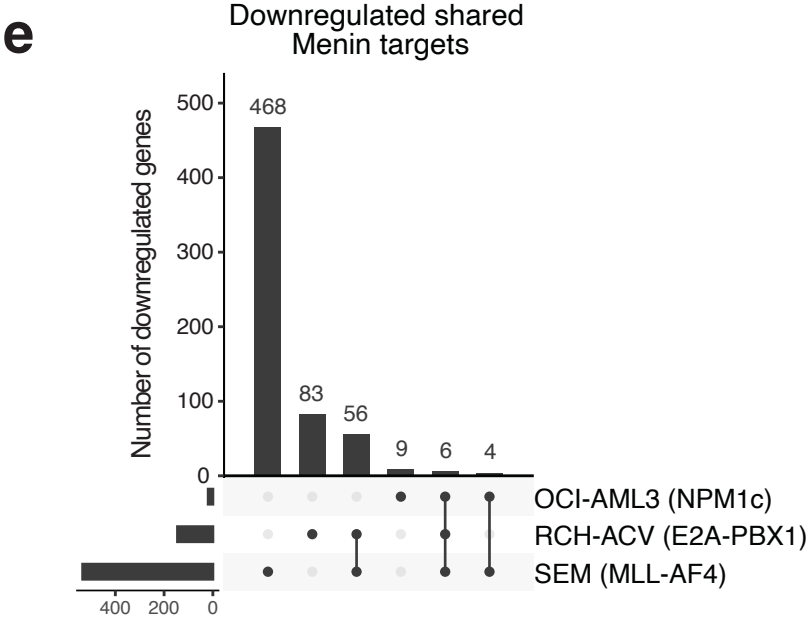

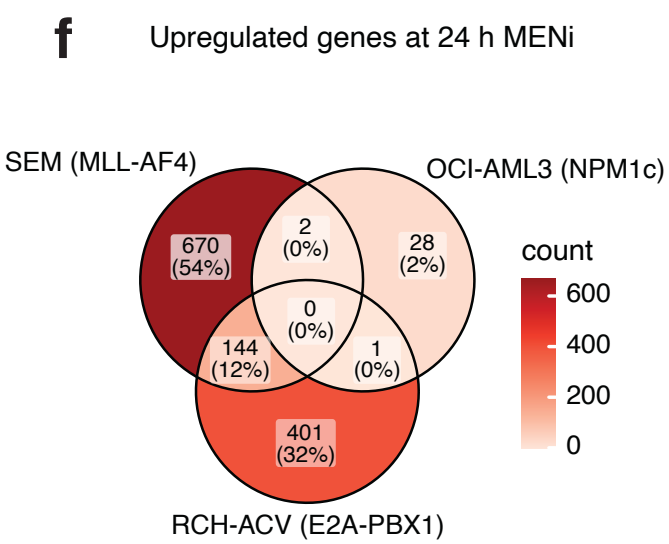

Continued on next page

Extended Data Figure 1 continued

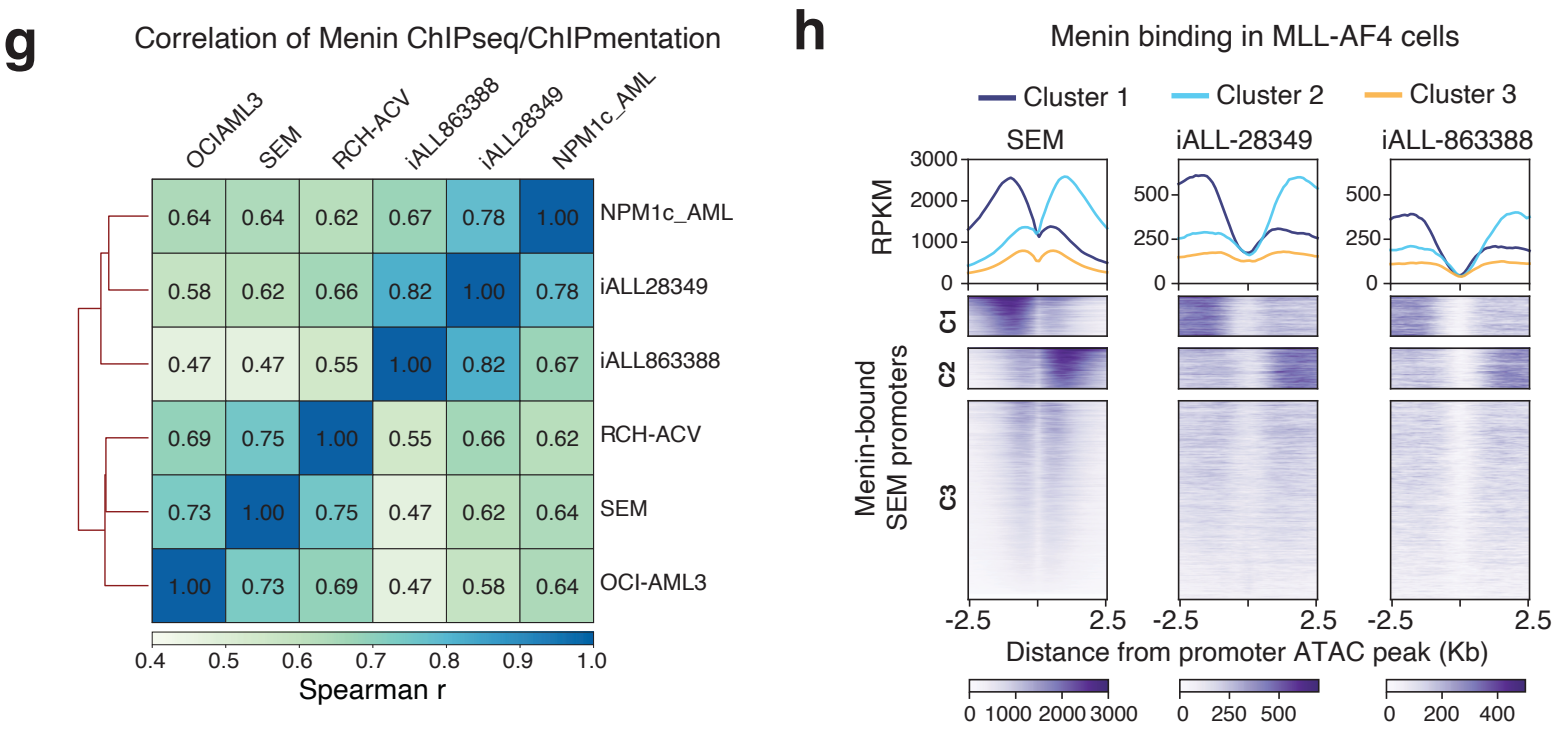

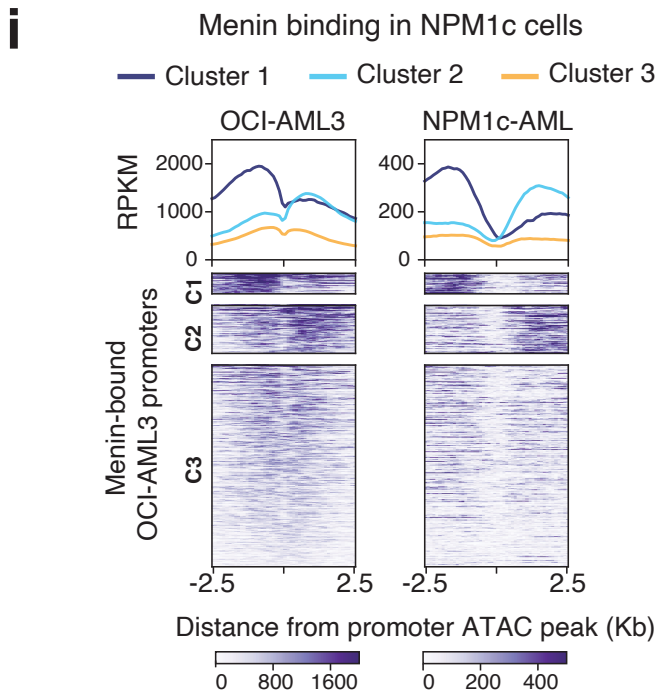

Extended Data Fig. 1 Association between Menin binding, cell viability, and transcription changes.

a, Menin ChIP-seq after 24 h treatment with DMSO or 250 nM Menin inhibitor VTP50469 (MENi) in SEM, RCH-ACV and OCI-AML3 cells. Metaplots show mean reference normalized reads per million (RRPM) centered on transcription start sites (TSS) genome-wide. **b**, Dose response curves to MENi recorded at 48 h using CellTiterGlo (n = 5 for SEM and RCH-ACV cells, n = 3 for OCI-AML3 cells). **c**, Colony forming units recorded after culture in Menin inhibitor (n=5). Error bars represent standard error. **d**, Violin plots depicting the log2 fold changes of differentially expressed genes (FDR < 0.05) after 24 h MENi (250 nM), split by Menin binding at the promoter. **e**, Upset plot representing the cell lines in which shared Menin-bound genes (centre of Venn diagram in Fig. 1d) are downregulated following MENi (250 nM) for 24 h. **f**, Intersections of all upregulated genes following 24 h MENi (250 nM) in SEM, OCI-AML3, and RCH-ACV cells. **g**, Correlation heatmap of genome-wide Menin ChIP-seq signal in cell lines (SEM, RCH-ACV, and OCI-AML3) and Menin ChIPmentation in primary patient samples (NPM1c-AML, iALL28349, iALL863388). **h**, Heatmaps and metaplots showing the mean Menin signal at promoters in SEM cells (ChIP-seq) and two primary patient samples (ChIPmentation), sorted and k-means clustered by Menin signal in SEM cells. **i**, Heatmaps and metaplots showing the mean Menin signal at promoters in OCI-AML3 cells (ChIP-seq) and one primary patient sample (ChIPmentation), clustered by Menin signal in OCI-AML3 cells.

Extended Data Figure 2

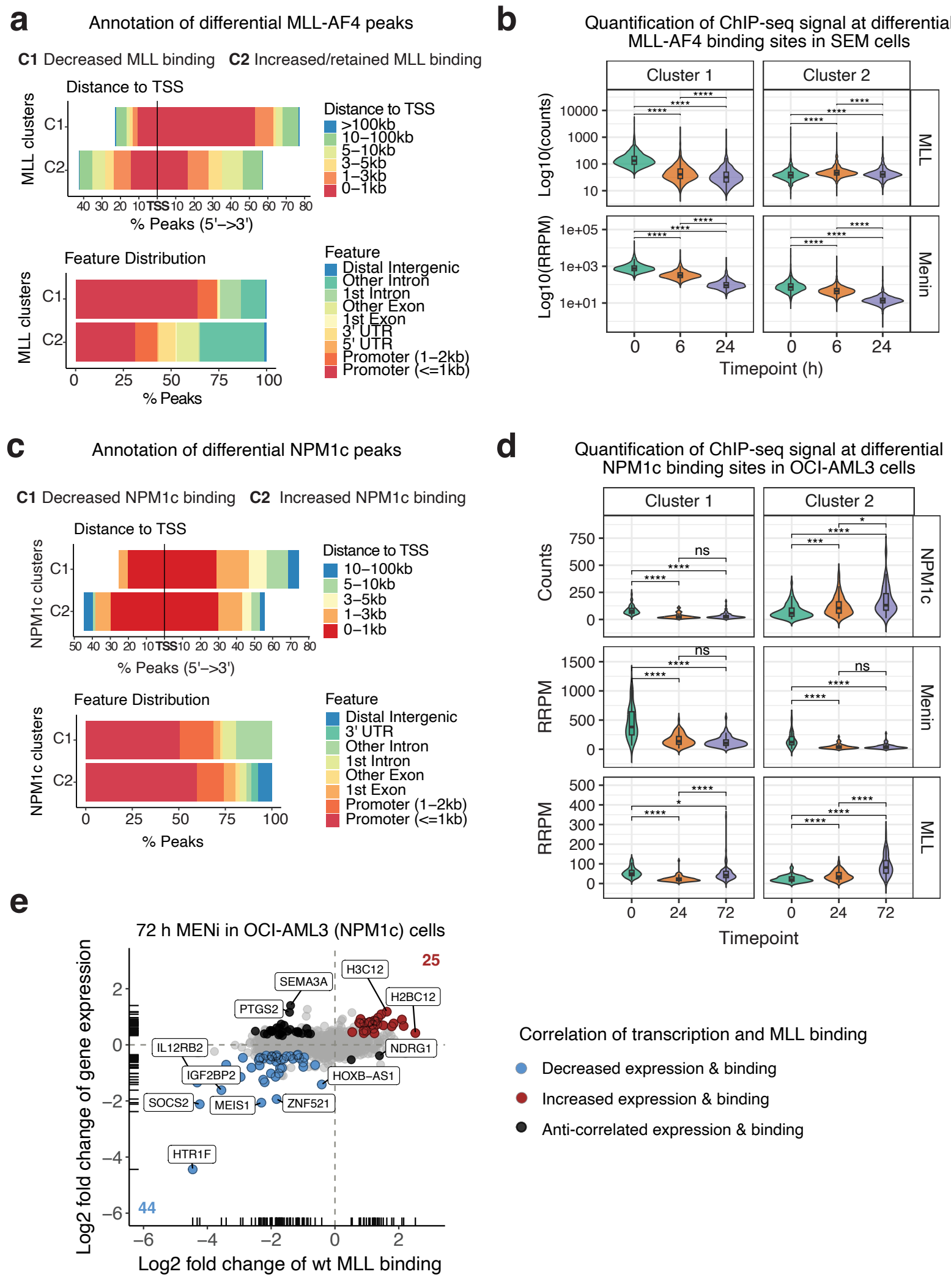

Extended Data Fig. 2 Changes in MLL/MLL-AF4 and NPM1c binding correlate with transcription changes at a subset of genes sensitive to MENi.

a, Annotation of differential MLL/MLL-AF4 peaks in SEM cells over a time course of MENi based on distance to TSS (top) and genomic features (bottom). **b**, Violin plots of MLL and Menin ChIPmentation signal at differential MLL/MLL-AF4 peaks in SEM cells. Pairwise comparisons from a Wilcoxon Test with Bonferroni-adjusted *p*-values are shown (ns: $p > 0.05$, *: $p<0.05$, **: $p<0.01$, ***: $p<0.001$, ****: $p<0.0001$). **c**, Annotation of differential NPM1c peaks in OCI-AML3 cells over a time course of MENi based on distance to TSS (top) and genomic features (bottom). **d**, Violin plots of NPM1c, Menin, and MLL ChIPmentation signal at differential NPM1c peaks in OCI-AML3 cells (Wilcoxon Test with Bonferroni-adjusted *p*-values ns: $p > 0.05$, *: $p<0.05$, **: $p<0.01$, ***: $p<0.001$, ****: $p<0.0001$). **e**, Correlation between the log2 fold changes of gene expression and wild-type MLL ChIPmentatation signal at promoters in OCI-AML3 cells after 72 h of MENi (250 nM). Genes with statistically significant changes in both gene expression and MLL binding are colored based on the direction of change.

Extended Data Figure 3

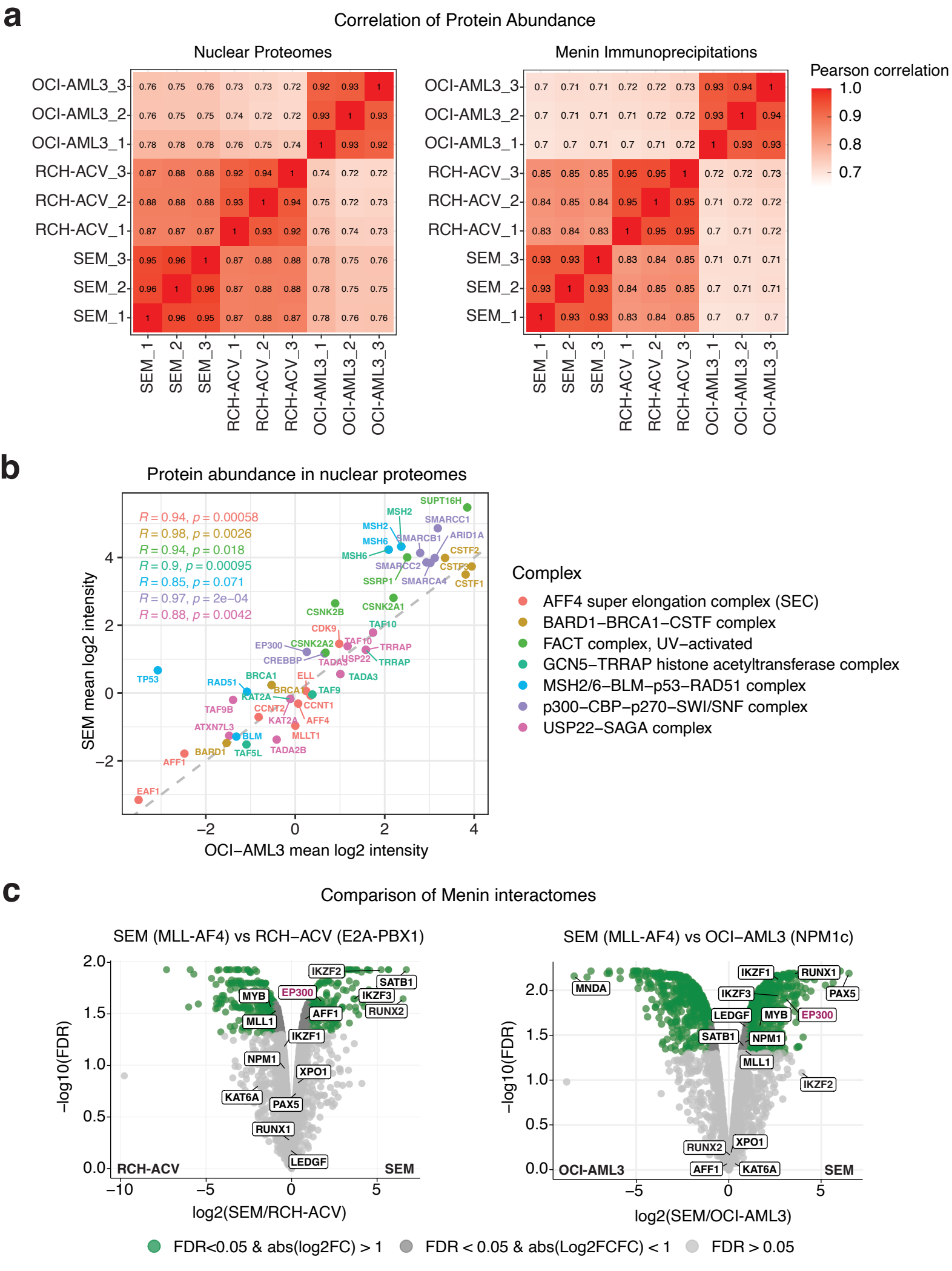

Extended Data Fig. 3 Menin co-IPs have different enrichments of transcription activators despite highly correlated interactomes and nuclear proteomes between cell lines.

a, Pearson correlations between nuclear proteome samples (left) and Menin immunoprecipitation (IP) samples (right), computed on log2-transofrmed and imputed data. **b**, Correlation in the abundance of differentially enriched complex components in the nuclear proteomes of SEM and OCI-AML3 cells. The grey dashed line represents a slope of 1. Pearson *R* values are shown for each complex. **c**, Comparison of proteins enriched in Menin IPs in SEM versus RCH-ACV cells (left) and SEM versus OCI-AML3 cells (right). Only proteins that were statistically enriched over IgG controls in at least one cell line (FDR < 0.01) were included.

Extended Data Figure 4

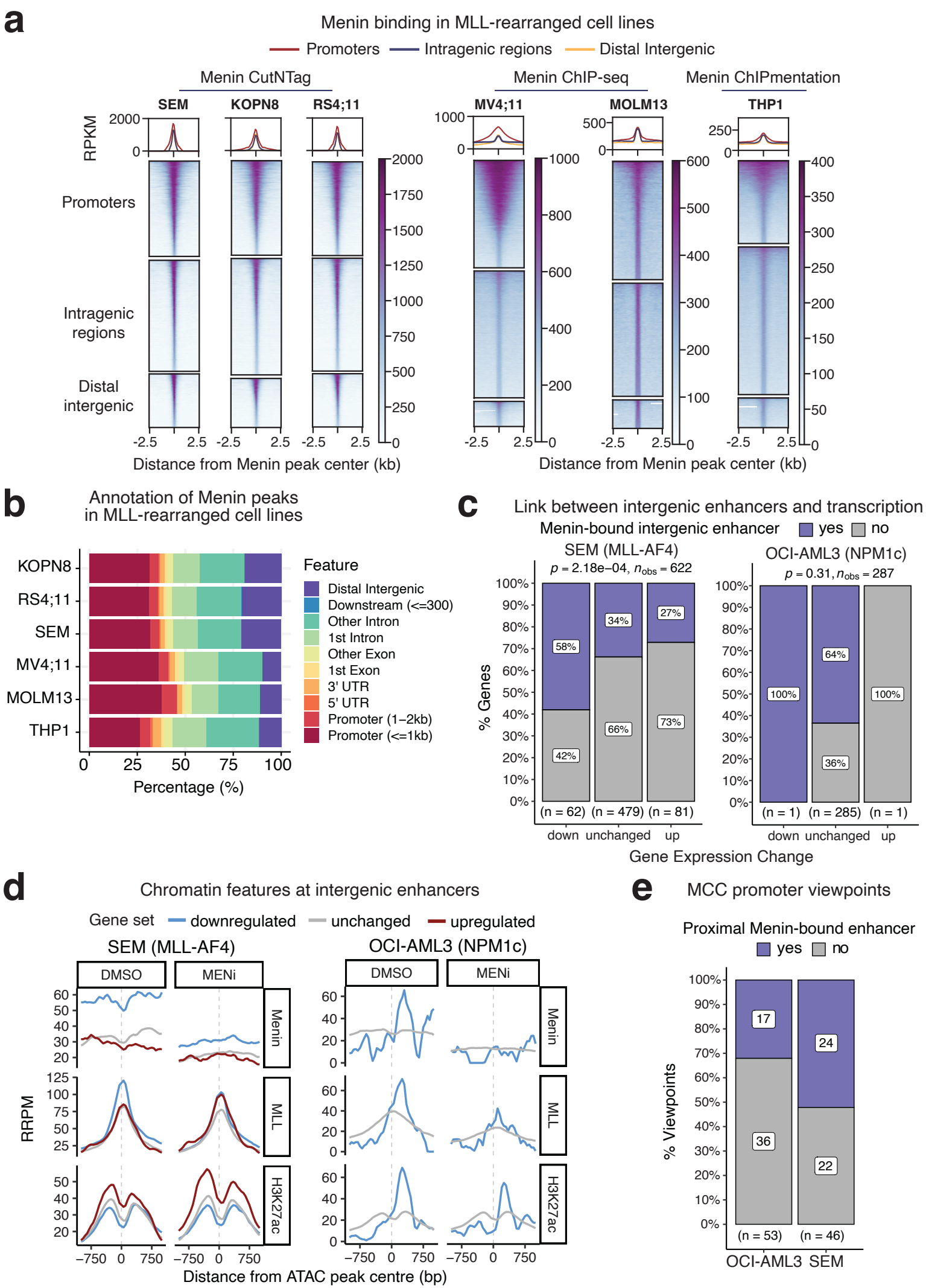

Extended Data Fig. 4 Menin binds enhancer elements.

a, Heatmaps and metaplots of mean Menin signal at promoters (±2 kb of a TSS), intragenic regions, and distal intergenic regions in cell lines with *MLL* translocations. **b**, Annotation of Menin peaks in cell lines with *MLL* translocations. **c**, Association between Menin binding at intergenic enhancers and gene expression following 24 h of MENi (250 nM). *p*-values are reported from a Pearson chi-squared test. **d**, Metaplots representing mean Menin, MLL, and H3K27ac signal at intergenic enhancers annotated to differentially expressed genes after 24 h of MENi (250 nM) in SEM and OCI-AML3 cells. **e**, Proportion of genes selected for Micro-Capture-C promoter viewpoints annotated with whether they have a proximal Menin-bound enhancer, assigned by nearest TSS.

Extended Data Figure 5

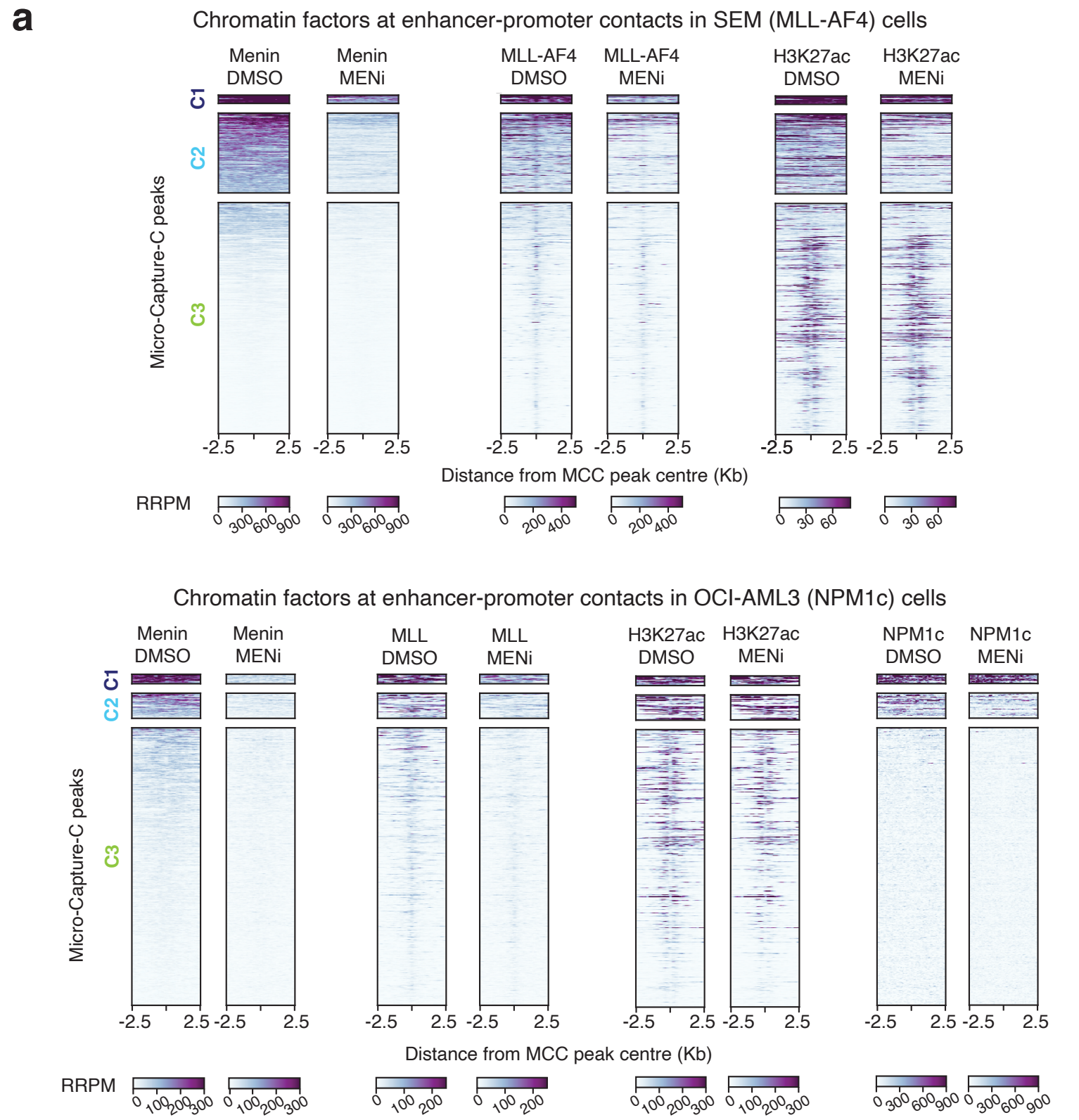

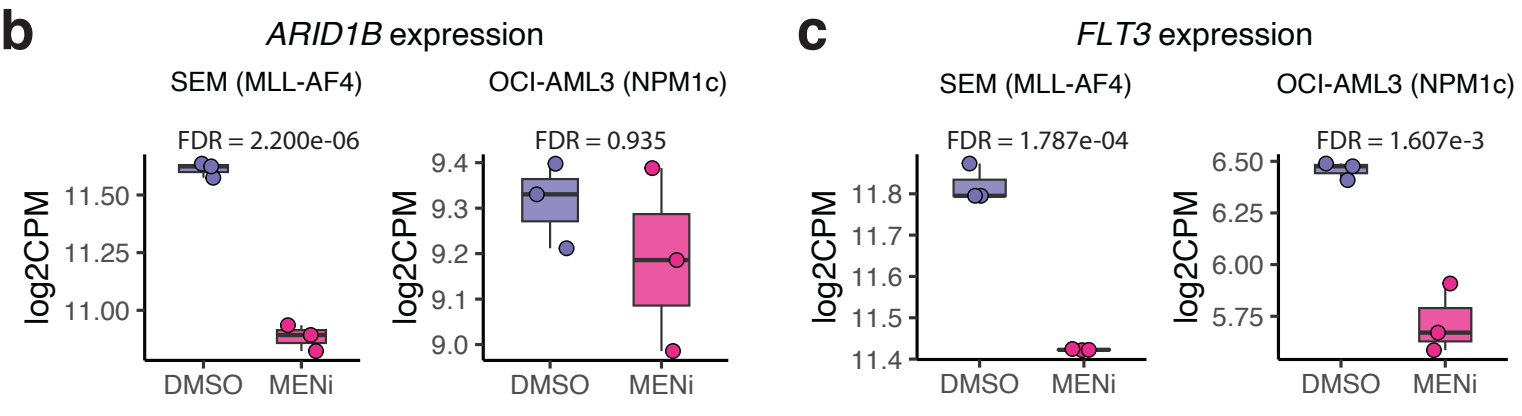

Extended Data Fig. 5 Menin binding regulates enhancer-promoter contacts in SEM but not OCI-AML3 cells.

a, Heatmaps of Menin, MLL/MLL-AF4, H3K27ac, and NPM1c signal at MCC peaks in SEM cells (top) and OCI-AML3 cells (bottom), clustered by Menin signal (k means = 3). **b**, Gene expression of *ARID1B* and **c**, *FLT3* in SEM and OCI-AML3 cells after 24 h DMSO or MENi (250 nM) treatment from TT-seq data (CMP = counts per million).

Extended Data Figure 6

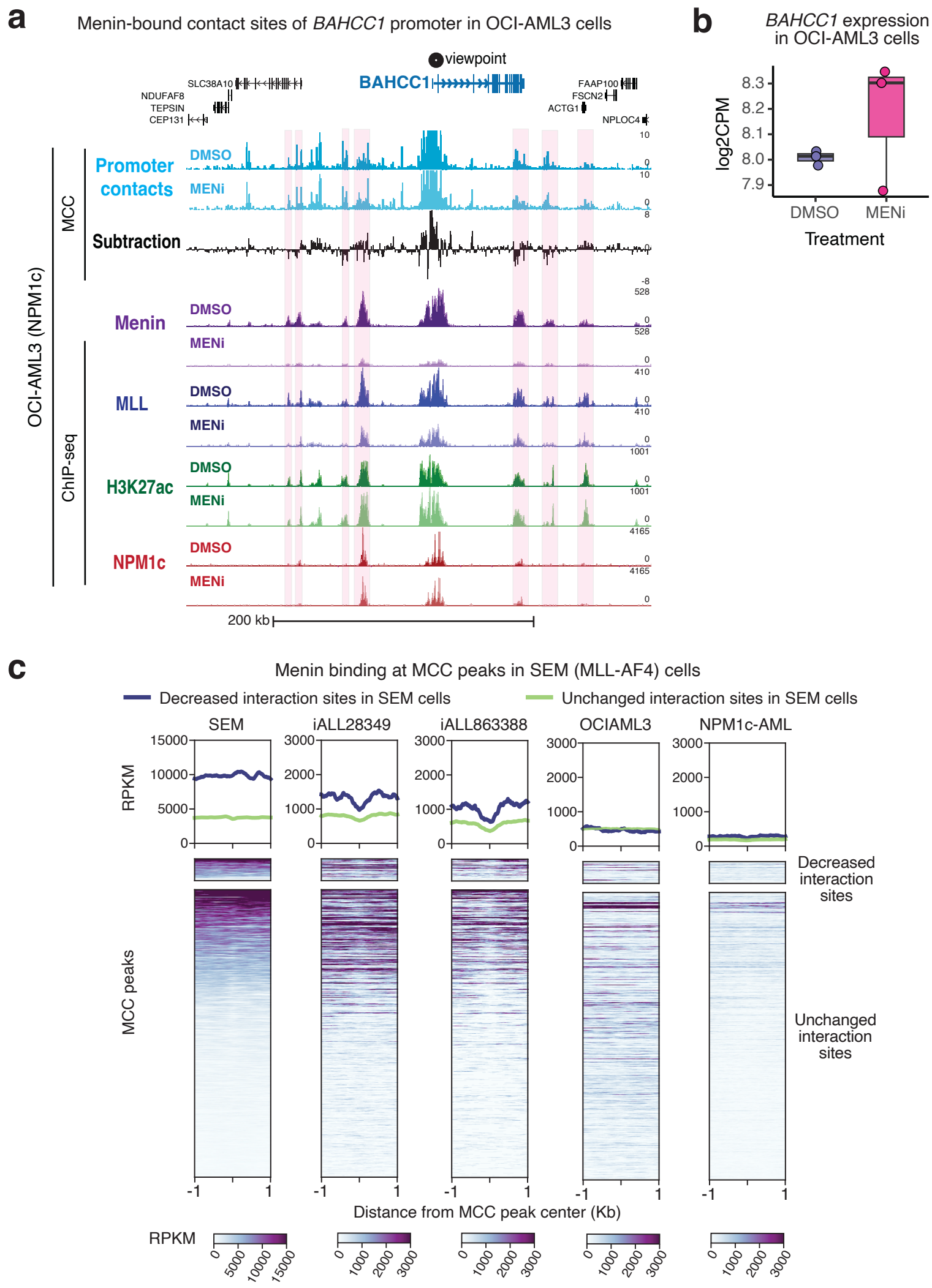

Extended Data Fig. 6 Menin is enriched at MENi-sensitive promoter contact sites in SEM cells and MLL-AF4 primary patient samples.

a, MCC and ChIP-seq for Menin, MLL, H3K27ac and NPM1c at the *BAHCC1* locus in OCI-AML3 cells. Menin-bound enhancer-promoter contacts are highlighted in pink. **b**, Gene expression of *BAHCC1* in OCI-AML3 cells after 24 h DMSO or MENi (250 nM) from TT-seq data (CPM = counts per million). **c**, Menin binding in cell lines (ChIP-seq in SEM and OCI-AML3 cells) and in primary patient cells (ChIPmentation in iALL28349, iALL863388, and NPM1c-AML) at MCC peaks in SEM cells. Menin signal at MCC peaks with a statistically significant (Mann Whitney U FDR q-value < 0.05, log2 fold change < 0) decrease in unique ligation junctions in SEM cells following MENi (250 nM, 24 h) is shown in dark blue on the metaplots and in the top cluster on the heatmaps.

Supplementary Table 1: Antibodies for chromatin immunoprecipitation

Antibody	Reference	Application (per 1 × 10^7 cells)
Menin	Bethyl A300-105A	2 μg for ChIP, 1 μg for IP
MLL N-terminus	Bethyl A300-086A	2 μg
H3K27ac	Diagenode C15410196	1.25 μg
H3K4me1	Diagenode C15410194	3 μg
H3K4me3	Diagenode C15410003	2.6 μg
NPM1c	ThermoFisher PA1-46356	2 μg
Rabbit IgG	Cell Signalling DA1E	1 ug

Supplementary Table 2: Sources of publicly available sequencing data

Dataset	Reference
OCI-AML3 ATAC-seq	GSM5114291
SEM Menin AutoCUTnTag	GSM5139719
KOPN8 Menin AutoCUTnTag	GSM5139645
RS4;11 Menin AutoCUTnTag	GSM5139689
iALL_28349 Menin ChIPmentation	GSM8657204
iALL_28349 H3K27ac ChIPmentation	GSM8657208
iALL_863388 Menin ChIPMentation	GSM8657184
iALL_863388 H3K27ac ChIPMentation	GSM8657191
MV4;11 Menin ChIP-seq	GSM5858383
MOLM13 Menin ChIP-seq	GSM3635683